

IMPACT OF DNA END STRUCTURE AND CELLULAR GROWTH PHASE ON
DNA REPAIR BY NONHOMOLOGOUS END-JOINING (NHEJ)
IN *SACCHAROMYCES CEREVISIAE*

by

O'Taveon R. Fitzgerald, B.S.

A thesis submitted to the Graduate Council of
Texas State University in partial fulfillment
of the requirements for the degree of
Master of Science
with a Major in Biochemistry
August 2020

Committee Members:

L. Kevin Lewis, Chair

Karen A. Lewis

Wendi David

COPYRIGHT

by

O'Taveon R. Fitzgerald

2020

FAIR USE AND AUTHOR'S PERMISSION STATEMENT

Fair Use

This work is protected by the Copyright Laws of the United States (Public Law 94-553, section 107). Consistent with fair use as defined in the Copyright Laws, brief quotations from this material are allowed with proper acknowledgement. Use of this material for financial gain without the author's express written permission is not allowed.

Duplication Permission

As the copyright holder of this work I, O'Taveon R. Fitzgerald, authorize duplication of this work, in whole or in part, for educational or scholarly purposes only.

ACKNOWLEDGEMENTS

I would like to thank all the people whose assistance proved instrumental to the completion of this project. My sincerest gratitude to my committee chair and research advisor Dr. Kevin Lewis, who has provided me extensive guidance and knowledge throughout my undergraduate and graduate academic career in pursuit of my professional goals. As my teacher and mentor, he has taught me the critical skills necessary to thrive in research. By his example I have been shown what a great scientist should be, and I am truly grateful to have had the opportunity to begin my research in your laboratory. Thank you to my committee, Dr. Karen Lewis and Dr. Wendi David, for your invaluable personal and professional guidance throughout my academic journey. I would also like to express my appreciation for my laboratory colleagues for their contributions and support through this research project, including Shubha Malla, Corbin England, and Sam Oliveira. This appreciation also extends to my graduate cohort for their help in sustaining a positive and supportive atmosphere. I am most thankful for my wife, Dioselina, whose immense love and support has kept me going through this project. I would also like to thank my mother Michelle, my grandparents Dorothy and James, and my siblings Alethea, Tametra, and Terry. I would not have been able to make it this far without all your love and support.

TABLE OF CONTENTS

	Page
ACKNOWLEDGEMENTS.....	iv
LIST OF FIGURES.....	vi
CHAPTER	
I. INTRODUCTION.....	1
II. MATERIALS AND METHODS.....	8
III. RESULTS AND DISCUSSION.....	21
IV. SUMMARY AND CONCLUSIONS.....	61
REFERENCES.....	67

LIST OF FIGURES

Title	Page
1. Mechanism of homologous recombination in yeast.....	4
2. NHEJ pathway involving three primary protein complexes.....	5
3. Transformation of plasmid DNA into yeast cells.....	21
4. Diagram detailing plasmid repair pathways.....	22
5. Diagram of NHEJ accuracy assays.....	23
6. Normalizing of plasmid transformation efficiency vs repair efficiency.....	24
7. Comparison of unmodified and modified transformation protocol.....	25
8. Comparison of transformation efficiency when using low or high molecular weight carrier DNA.....	26
9. Comparison of transformation efficiencies using different DMSO concentrations.....	27
10. NHEJ repair efficiency of wildtype cells compared to <i>dnl4</i> mutants.....	28
11. Diagram of pRS315URA3 plasmid.....	29
12. A 0.8% agarose gel electrophoresis showing <i>NcoI</i> digestion of the pRS315URA3 plasmid.....	30

13. Different NHEJ repair complex requirements in early stationary <i>MATα</i> <i>S. cerevisiae</i> cells.....	32
14. Early stationary phase NHEJ mutation frequency comparison of <i>MATα</i> <i>dnl4</i> , <i>yku70</i> , and <i>mre11</i> mutants.....	34
15. Percentage of G ₁ cells in cell growth phases compared with requirement for Mrx complex in NHEJ repair.....	35
16. NHEJ repair efficiency for 5' overhangs in mid-log phase <i>MATα</i> cells.....	36
17. NHEJ mutation frequencies for 5' overhangs in mid-log phase <i>MATα</i> strains.....	37
18. NHEJ repair efficiency of NcoI-cut pRS315URA3 in early stationary <i>MATα</i> cells.....	38
19. NHEJ mutation frequency in early stationary <i>MATα</i> cells.....	39
20. NHEJ repair efficiencies for 5' overhangs in mid-log phase <i>MATα</i> <i>dnl4</i> , <i>yku70</i> , and <i>mre11</i> mutants.....	40
21. NHEJ mutation frequencies for mid-log phase <i>MATα</i> <i>dnl4</i> , <i>yku70</i> , and <i>mre11</i> mutants.....	41
22. Percentage of unbudded (G ₁) vs budded (S + G ₂ /M) cells.....	43
23. pLKL67Y plasmid diagram.....	44
24. NHEJ efficiency assay using BmtI-digested pLKL67Y in early stationary phase <i>MATα</i> <i>dnl4</i> , <i>yku70</i> , and <i>mre11</i> mutants.....	45

25. NHEJ mutation frequencies for 3' overhangs in early stationary phase <i>MATα</i> cells.....	46
26. NHEJ repair efficiency of BmtI-digested pLKL67Y using mid-log phase <i>MATα</i> cells.....	47
27. NHEJ repair mutation frequencies in mid-log phase cells using BmtI-digested pLKL67Y.....	48
28. Repair efficiency reduction with different amounts of cut plasmid.....	49
29. Genomics screen identified new NHEJ repair mutants.....	50
30. NHEJ repair efficiency of <i>arp5</i> cells.....	51
31. Diagram of new pLKL103Y plasmid.....	52
32. BsmI-digestion of pLKL103Y.....	53
33. BsmI and SacI digestion of pLKL103Y visualized using 0.7% agarose gel electrophoresis.....	54
34. NHEJ vs HDR repair pathway choice using pLKL103Y.....	55
35. PCR mutagenesis of pLKL91Y to create pLKL104Y.....	57
36. PCR addition of BspMI sites and digestion of plasmid to create gap in <i>HIS3</i> gene.....	60
37. Diagram of cellular growth phases.....	62
38. Repair 5' versus 3' ssDNA overhangs in <i>Mrx⁻</i> cells.....	64

39. NHEJ vs HDR DSB repair assay diagram using new gapped plasmid system.....66

I. INTRODUCTION

The DNA within a cell is continuously subjected to damaging agents (DNA nucleases, radiation, free radicals, and other mutagens) that can cause different abnormalities in the chemical structure, potentially preventing replication and transcription mechanisms from functioning correctly ¹. This damage can happen in a variety of ways, including modifications of nucleotides, intra- and interstrand crosslinks, single-strand breaks (SSBs) and double-strand breaks (DSBs). Although there is a variance in severity, many lesions have the potential to inhibit various DNA processes. A particularly deleterious consequence is lack of fidelity in DNA replication, which can further propagate the DNA damage and lead to mutations, eventually resulting in cell death ². Therefore, different repair pathways/mechanisms are essential to maintain genome integrity during the proliferation of cells.

Different types of lesions utilize specific repair pathways with their own mechanisms and components required to repair DNA damage. The major repair pathways for eukaryotic cells are Nucleotide Excision Repair (NER; primarily for UV light-induced crosslinks), Base Excision Repair (BER; repairs modified bases, e.g., via oxidation, alkylation, or deamination) and the Mismatch Repair pathway (MMR; repairs mismatched bases) ^{3,4}. One potent form of DNA damage is the DSB, which can be caused by nucleases within the cell, arise during blockage of DNA replication forks or by exposure to chemical or physical mutagens. A few reasons for their deleterious effects are the difficulty in repairing this type of damage and that each incidence of a DSB can lead to loss of cellular function, death, or mutations⁵. This severity is one reason the cell

dedicates two specific pathways to repair them: Homologous Recombination (HR), also called Homology-Directed Repair (HDR), and Nonhomologous End-Joining (NHEJ). The pathways employ different mechanisms and protein complexes to repair DSBs, and they are conserved in all eukaryotes, including yeast and humans. Some consequences of inactivation of these DNA repair pathways due to mutations in the genes that encode the proteins involved are an increased cancer risk. Examples of this include the *BRCA1* and *BRCA2* genes involved in breast/ovarian cancer, *MSH* genes in colorectal cancer, and *ERCC* genes causing Xeroderma Pigmentosum, which leads to a predisposition to certain skin cancers (Table 1) ⁶⁻¹¹.

Table 1. Consequences of inactivated/ defective genes in DNA repair pathways.

Gene	Repair pathway	Cancer
BRCA1,2	HR	Breast, Ovarian
ERCC2,3,4,5	NER	Skin
NBN	NHEJ	Lymphoid
MRE11	HR + NHEJ	Leukemia, Lymphoma
MSH2,3,6	MMR	Colon

Despite the conserved nature of the pathways between humans and yeast, HR is the preferred pathway in yeast and NHEJ is preferred in humans for DSB repair. HR uses homologous regions of chromosomes as a template when repairing DSBs. The pathway of choice is dictated by factors such as the presence of certain proteins (e.g. Rif1 in humans) and the cell-cycle phase ¹²⁻¹⁵. One determining factor of pathway choice is the

resection of the DSB via exonuclease activity to form long single-strand DNA (ssDNA) tails. After resection has occurred, the HR pathway will be utilized in the repair of the DSB¹⁶. Rif1 plays a role in the mediation of pathway choice by acting as an antagonist to the irreversible end-resection by protecting the exposed ssDNA ends and favoring NHEJ repair¹⁷. Two of the primary protein complexes in yeast HR are the Mrx complex (Mre11, Xrs2, Rad50) composed of the Mre11 nuclease, along with the Rad50 and Xrs2 proteins that promote structural stability and support in binding the target DNA ends, and other members of the RAD52 group of proteins (Rad51, Rad52, Rad54, Rad55, Rad57 and Rad59)¹⁸⁻²⁰. The latter proteins are exclusive to HR, but the Mrx complex is involved in both HR and NHEJ. HR begins with resection by Mrx and Sae2 to produce short 3' ended ssDNA tails, then the DNA is resected further by Exo1 and Sgs1-Dna2 and the long ssDNAs are coated with Rpa (ssDNA binding protein) (Figure 1). Next, Rad51 and Rad52 initiate strand invasion with the 3' ssDNA tails into the homologous region of another chromosome to form a D-loop structure and begin the synthesis of new DNA^{21,22}. While this is occurring the second DSB end can be "captured", forming an intermediate structure made up of two Holliday junctions, and DNA is synthesized and ligated to form a continuous structure. The resolution of these junctions is mediated by specialized endonucleases called resolvases that can produce either non-crossover (less common) or crossover repaired DNA products²³.

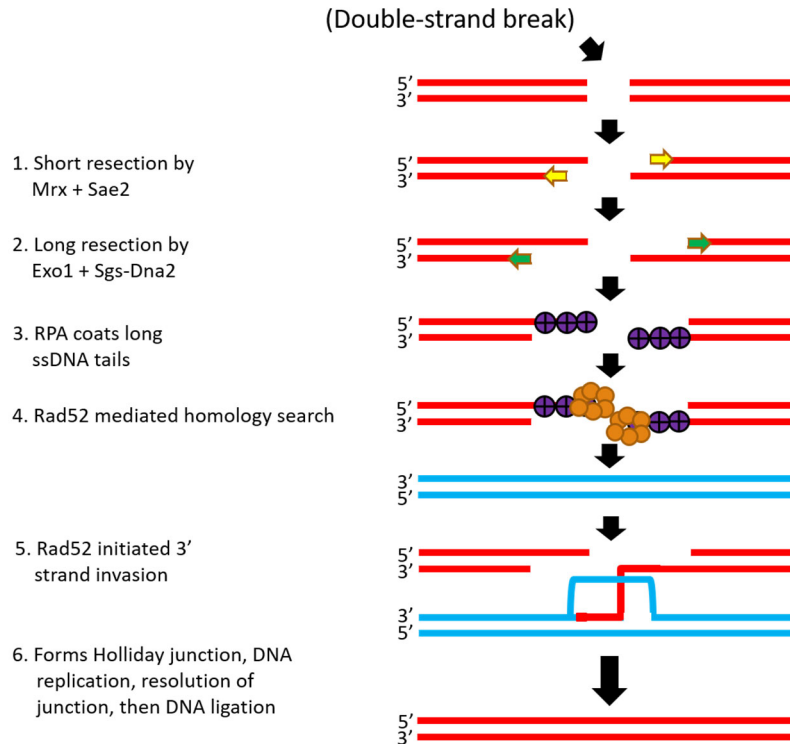


Figure 1. Mechanism of homologous recombination in yeast.

The second pathway, and the focus of this project, is the NHEJ pathway (Figure 2). This process is initiated when the Ku protein complex (Yku70-80 in yeast), along with other structurally supporting proteins (e.g. DNA-dependent protein kinase) binds non-specifically to the ends of the DSB, not allowing nucleases to degrade the ends²⁴⁻²⁸. While acting as structural support in keeping the broken strands in proximity, the Ku complex still allows for the access to the DNA strands, while recruiting the Mrx and DNA Ligase IV complexes²⁹. The next complex is Mrx (Mre11-Rad50-Xrs2), which in NHEJ repair binds to the Yku/DNA complex and tethers the broken DNA ends. The presence of the additional proteins inhibits the nuclease activity of Mrx and other nucleases, allowing NHEJ repair to proceed^{12,14}. The third and final NHEJ complex, DNA ligase IV (Dnl4, Lif1, Nej1), ligates the two broken ends to repair the DSB^{30,31}.

Although NHEJ is not the primary repair pathway in yeast, in G₁ phase it is the predominant pathway due to the lack of homologous chromosomes (sister chromatids) required to complete HR³². Other factors that play a role in the efficiency of DNA repair by NHEJ are chromatin remodeling (e.g., RSC (Remodel the Structure of Chromatin) complex) that facilitates access of repair proteins to the DSBs, DNA damage-associated cell cycle checkpoints (e.g., Mec1, Ddc2, Rad9, Rad53, etc.) to allow time for repair, and the processing of the ssDNA tails to allow for successful ligation of the broken ends (e.g., Rad1, Rad10, Mus81, Mms4, etc.)³³⁻³⁸.

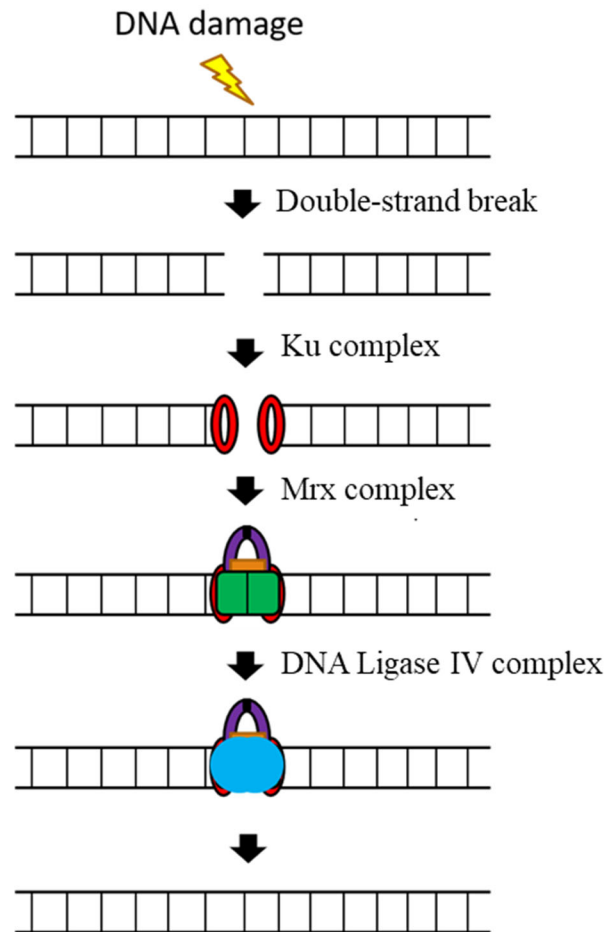


Figure 2. NHEJ pathway involving three primary protein complexes.

Previous work suggested that each NHEJ protein complex plays an essential role in the repair pathway^{32,39-41}. However, no more than three NHEJ genes have ever been tested in a single study, and no previous reports have tested the genes encoding all the complexes (Yku, Mrx, and Dnl4). A recent study in our lab utilized plasmid DNA assays to test repair efficiency and accuracy in cells with mutations in each of the eight genes involved in the NHEJ pathway⁴². Also, the study analyzed various types of DSB structures (5' vs 3' overhangs). Repair of DSBs in Yku and DNA ligase IV complex mutants was strongly decreased, regardless of the end structures of the DSBs. By contrast, repair in Mrx mutants was not strongly reduced for DSBs with 5' ssDNA overhangs but was decreased for repair of breaks with 3' ssDNA overhangs. These results suggest that Mrx plays a less significant role in the repair pathway than the other two complexes under some conditions. Another previous graduate student Jennifer Lilley performed a genomics screen of a yeast mutant library and identified three genes (*ARP5*, *BUD32*, and *MCT1*) that caused a reduction in NHEJ repair efficiency when inactivated in both *MATa* and *MATα* haploid yeast strains⁴³. This screen also identified 3 genes that affected the NHEJ repair accuracy (*LSM7*, *RTF1*, and *MCT1*). These genes, although not directly associated with the three main NHEJ complexes, might play an important role in efficient and accurate (mutation-free) NHEJ repair⁴⁴⁻⁴⁶.

The goals of this project were to expand upon these findings and see how different forms of DNA overhangs change the efficiency and accuracy of NHEJ. The goal of the initial experiments was to test several potential improvements to the chemical-based yeast transformation protocol used for plasmid NHEJ repair assays⁴⁷. This was accomplished via optimization of the average bp size of the sonicated salmon sperm

carrier DMSO concentration was for cell wall solubilization, and concentration of digested plasmid DNA that resulted in the most pronounced efficiency reduction contrast between the mutant strains tested.

A second goal was to see the effects that the cellular growth phase (early stationary compared to mid-log phase) would have on the requirement for the Mrx complex in efficient NHEJ repair. Results indicated that the cellular growth phase did play a role in the requirement for the Mrx complex, depending on the DNA end structure.

The third goal was to characterize the new mutants identified by Jennifer Lilley (particularly the Arp5 protein) and determine their roles in NHEJ, HR, and DNA damage checkpoints. The final goal of this project was to create a novel method of plasmid transformation that would enable the analysis of repair proficiency by both DSB repair pathways (NHEJ and HDR) simultaneously. This was first done via the creation of a new plasmid, pLKL103Y, that could be repaired by either pathway after transformation into yeast cells. To further analyze this distinction, a new method was designed to create a gapped plasmid using PCR and Type IIS restriction enzymes. This new system was designed to have a flexible amount of homology around the gap for a greater ability to use HDR and NHEJ for repair.

II. MATERIALS AND METHODS

Materials

Chemical reagents and instruments

Amino acids (adenine, uracil, histidine, leucine, lysine, and tryptophan), lithium acetate (LiAc), dimethyl sulfoxide (DMSO), ampicillin, and RNase A were purchased from Sigma-Aldrich Chemical Co. (St. Louis, MO). 1 kb and 2-log DNA ladder, NcoI, BsmI, BmtI, SacI, and 10X CutSmart buffer were purchased from New England Biolabs (Ipswich, MA). Polyethylene glycol-4000 (PEG) was supplied by Fluka Analytical. EDTA was supplied by Omnipur (Darmstadt, Germany). Ethidium bromide (EtBr) was purchased from IBI Scientific (Peosta, IA). D-glucose (dextrose), ammonium sulfate, sodium dodecyl sulfate (SDS), and soy peptone were purchased from VWR (Radnor, PA). Agar and LB agar media were purchased from Teknova (Hollister, CA). BD Bioscience (San Jose, CA) supplied Bacto yeast extract. Sonicated salmon sperm carrier DNA was purchased from Invitrogen (Carlsbad, CA). 50X TAE was purchased from MP Biomedicals (Solon, OH). The Alpha Innotech Red imager was supplied by ProteinSimple (San Jose, CA). Qubit 2.0 Fluorimeter was purchased from Thermo Fisher Scientific (Waltham, MA). Applied Biosystems supplied the 2720 Thermal cycler (Foster City, CA).

Yeast Strains and plasmids

Yeast strains for this project were derived from BY4742 (*MAT α ura3- Δ 0 leu2- Δ 0 lys2- Δ 0 his3- Δ 1*) and BY4741 (*MAT α ura3- Δ 0 leu2- Δ 0 met17- Δ 0 his3- Δ 1*) and have been

described⁴⁸. Genotypes of derivative strains are as follows: YLKL857 (as BY4742, *yku70Δ::G418^r*), YLKL650 (as BY4742, *mre11Δ::G418^r*), YLKL858 (as BY4742, *dnl4Δ::G418^r*), YLKL1637 (as BY4741, *yku70Δ::G418^r*), YLKL1636 (as BY4741, *mre11Δ::G418^r*), YLKL1533 (as BY4741, *dnl4Δ::G418^r*).

The plasmids used for NHEJ repair efficiency and accuracy experiments, pRS315URA3 (*CEN/ARS LEU2 URA3*) and pLKL67Y (*2μ URA3 HIS3*) were obtained from the Lewis laboratory DNA collection. The pLKL91Y (*CEN/ARS LEU2 HIS3*) plasmid used in the creation of pLKL103Y was also obtained from the Lewis laboratory. pRS313 (*CEN/ARS HIS3*), pRS315 (*CEN/ARS LEU2*), and pRS316 (*CEN/ARS URA3*) have been described⁴⁹.

Yeast and E. coli growth media

Yeast cells were grown on YPDA plates (1% w/v bacto yeast extract, 2% w/v soy peptone, 2% w/v glucose (dextrose), 2.2% w/v bacto agar, and 0.5% adenine) for non-selective cultivation. YPDA broth for overnight cultures was prepared similarly to YPDA plates, excluding agar. Synthetic glucose plates (0.5% w/v ammonium sulfate, 0.17% w/v yeast nitrogen base, 2% w/v glucose (dextrose), 2.2% w/v agar, and .051% 10 amino acid mix) contained necessary amino acids and bases except histidine, leucine or uracil that were selectively excluded for discriminatory growth. *E. coli* cells were grown on LB with ampicillin plates that contained 1% w/v tryptone, 0.5% w/v yeast extract, 1% w/v sodium chloride, 1.5% w/v agar and 100 μg/mL ampicillin. Bacterial cells were cultured in LB24 broth (1% w/v tryptone, 2.4% w/v yeast extract, 0.5% w/v NaCl, and 0.1% v/v 1 M NaOH).

Methods

Gel electrophoresis

Gel electrophoresis was done using 0.7%-1.4% w/v agarose gels in 1X TAE (40 mM Tris base, 20 mM acetic acid, 1 mM EDTA) running buffer at ~130 V using Life Technologies Horizon gel rigs. The gels were stained using 0.5 mg/mL ethidium bromide (EtBr) for 15 min, then imaged using an Alpha Innotech Red gel imager from ProteinSimple (San Jose, CA).

Early stationary phase yeast cell transformation

Early stationary phase cell transformation of plasmid DNA was performed using a modified version of the protocol described by Tripp *et al.*⁴⁷. Modifications were enacted to increase transformants per microgram of DNA and produce more transformant colonies from mutant strains exhibiting inadequate uptake of plasmid DNA. The protocol was performed as described:

1. Centrifuge 1.0-1.5mL (per assay tube) of an overnight liquid culture of cells at 2500xg for 15 s and then discard the supernatant.
2. To the cell pellet, add ~506 μ L of a master mix containing: 800 μ L 50% PEG, 100 μ L 1 M LiAc, 20 μ L 50 mM EDTA, 10 μ L 1 M Tris (pH 7.5), 70 μ L deionized water, 5 μ L 10 mg/mL boiled sonicated carrier DNA, and 1-10 μ L plasmid DNA per assay and vortex to resuspend. The master mix contains enough volume to complete all transformations plus one extra transformation.
3. Add 1/10th volume of DMSO (~ 56 μ L) and vortex to mix.
4. Incubate at 30 °C for 20 min.

5. Incubate at 42 °C for 20 min (8 min for temperature sensitive mutants e.g. *yku70* cells).
6. Centrifuge at 2500xg and remove supernatant. Pipette to resuspend cells in 1 mL of YPDA broth and incubate for 40 min at 30 °C with shaking. Centrifuge cells at 2500xg for 15 s, discard supernatant, add 200-800 µL deionized water, and resuspend with pipetting.
7. Spread a 10-100 µL aliquot onto selective plates. To optimize spread coverage, when adding less than 50 µL, spot 50-100 µL water to the center of the plate and pipette cells directly into the water, then spread.
8. Incubate plates at 30 °C for ~ 3 days or room temperature for 4-5 days.

Mid-log phase yeast cell transformation

For mid-log phase yeast cell transformations, the modified Tripp *et al.* protocol previously described was used with additional modifications to ensure utilization of a 3.0×10^6 cells/mL initial culture. The protocol was performed as follows:

1. Using a sterile toothpick, put a large blob of cells from a YPDA plate into 400 µL YPDA broth in a 1.5 mL microcentrifuge tube and vortex 4-5 s.
2. Dilute cells 1/50 into 1 mL water then vortex and sonicate for 15 s at 24% amplitude.
3. Load hemacytometer with ~12 µL diluted cells and take an average count of three separate squares.
4. Calculate cell titer by multiplying (average number of cells per square) x (25 total squares) x (50/1 dilution factor) x (10,000 hemacytometer multiplication factor).

5. Divide desired cell count (3.0×10^6) by new titer calculated and multiply by 1,000 for mL of cells to be added for 3.0×10^6 total cells.
6. Aliquot calculated amount to cells in microcentrifuge tubes and incubate at $30\text{ }^\circ\text{C}$ with shaking for ~ 6 h.
7. Centrifuge cells for 5 min at $2500\times g$ and discard supernatant.
8. Resuspend in 1 mL of 0.1 M LiAc and transfer to a 1.5 mL tube.
9. Add 351 μL of master mix solution containing: 240 μL 50% PEG, 36 μL 1 M LiAc, 5 μL 10 mg/mL boiled sonicated carrier DNA, 70 μL total of water and plasmid DNA. Make enough for all transformations plus an additional transformation.
10. Vortex to resuspend and add $1/10^{\text{th}}$ volume DMSO to the mixture and vortex again.
11. Shake at $30\text{ }^\circ\text{C}$ for 20 min.
12. Heat shock at $42\text{ }^\circ\text{C}$ for 20 min (8 min for heat sensitive strains).
13. Centrifuge for 15 s at $2500\times g$ and remove supernatant.
14. Resuspend cells in 200-800 μL water and spread 5-200 μL aliquots onto selective media. To optimize spread coverage, when adding less than 50 μL , spot 50-100 μL water to center of the plate and pipette cells directly into the water, then spread.
15. Incubate plates at $30\text{ }^\circ\text{C}$ for 3 days.

E. coli plasmid minipreps

Overnight cultures of *E. coli* cells were grown in 2-5 mL of LB24 broth plus 100 $\mu\text{g/mL}$ ampicillin shaking overnight at $37\text{ }^\circ\text{C}$. 1.5 mL of the culture were transferred to

microcentrifuge tubes and centrifuged at 17,000xg for ~15 s. The supernatants were discarded, and the bacterial pellets were resuspended in 100 μ L of an ice-cold solution of 50 mM glucose, 25 mM Tris (pH 8.0), and 10 mM EDTA (pH 8.0) by scraping the bottom of the tubes against a test tube rack until thoroughly mixed. 200 μ L of a freshly prepared solution of 0.2 M NaOH and 1% SDS was added, followed by mixing by inverting the tubes rapidly 5-6 times and allowing them to sit for 1 min. 150 μ L of an ice-cold solution of 3 M KOAc was added to the microcentrifuge tubes and they were inverted vigorously to mix, then stored on ice for 3 min. Tubes were then centrifuged at 21000xg for 10 min to sediment cell debris and proteins. The resulting supernatants were transferred to clean microcentrifuge tubes, avoiding the pellet below. DNA was precipitated by adding 400 μ L isopropanol to the microcentrifuge tubes, inverting several times to mix, and centrifuging at 21000xg for 3 min. The supernatants were discarded and 500 μ L of cold 70% ethanol was added, and tubes were centrifuged at 21000xg for 2 min. After discarding the supernatants, the microcentrifuges tubes were put upside down on a layer of 3 Kimwipes to dry for 60 min. The dry pellets were resuspended in 50 μ L TE and 1 μ L of 2 mg/mL RNase A and incubated at room temperature for 15 min, and then stored at -20 $^{\circ}$ C.

E. coli plasmid midipreps

E. coli plasmid midipreps were performed similarly to the previously described *E. coli* plasmid miniprep protocol. The modifications to the miniprep protocol are primarily in the amount of reagents used throughout the process. The protocol was performed as follows:

1. Use a toothpick to pick up a swath of *E. coli* cells from a streaked LB plus ampicillin plate and transfer cells to 0.5 mL of LB24 broth in a 1.5 mL microcentrifuge tube and rotate toothpick against the side to remove cells. Vortex tube and pipette cells into 100 mL LB24 broth plus 100 ug/mL ampicillin and shake overnight at 37 °C.
2. Transfer 45 mL of overnight culture into two 50 mL conical tubes and centrifuge them at 5,000xg for 4 min at 4 °C in Sorvall Lynx 6000 centrifuge.
3. Discard supernatant and add 1.5 mL of a cold solution of 50 mM glucose, 25 mM Tris (pH 8.0), and 10 mM EDTA (pH 8.0) by pipetting until mixed and keep on ice.
4. Add 3 mL of freshly prepared room temperature solution of 0.2 M NaOH and 1% SDS and mix by inverting the tubes rapidly, then store tubes at room temperature for 0.5 min.
5. Add 2.5 mL of an ice-cold solution of 3 M KOAc and invert tube vigorously to mix and store on ice for 5 min.
6. Centrifuge at 15,000xg for 5 min to sediment proteins and *E. coli* chromosomal DNA, and transfer supernatant to new 50 mL conical tubes
7. Precipitate DNA by adding 6 mL isopropanol and inverting several times vigorously. Centrifuge tubes for 2 min at 14,000xg at 10 °C.
8. Remove supernatant from white DNA and RNA pellet, add 7 mL of 70% ethanol and let sit for 2 min.
9. Pour off the ethanol wash and invert the tubes on 3 layers of Kimwipes and allow to dry for at least 30 min. To the dry pellets, add 0.8 mL of TE plus 10 µL of 2

mg/mL RNase A and incubate at room temperature for 10 min. Flick tubes to fully dissolve pellet.

10. Transfer liquids to 1.5 mL microcentrifuge tubes, centrifuge at 14,000xg for 1 min and transfer to new 1.5 mL tubes. Store at -20 °C.

E. coli transformation

1. Obtain frozen Top 10 competent *E. coli* cells and thaw on ice for 10 min.
2. Place 100 μ L of thawed competent cells into 1.5 mL microcentrifuge tube and add 100 μ L of cold KCM (100 mM KCl, 30 mM CaCl₂, 50 mM MgCl₂) then flick to mix the contents.
3. Place tube on ice for 15 min.
4. Immerse the lower half of the tubes in room temperature (30 °C) for 10 min.
5. Add 0.9 mL of LB24 broth and incubate with shaking for 50 min.
6. Centrifuge cells at 17,000 xg for 0.5 min, discard the supernatant, then add 200 μ L LB24 broth then vortex to resuspend.
7. Spread two separate aliquots of 30 μ L and 150 μ L to LB + Amp plates, then allow cells to grow for 24 h. Store at 4 °C.

Plasmid DNA restriction digests

pRS315URA3 was digested with the restriction enzyme NcoI (10,000 U/mL) to induce a 5' DSB with a 4-nucleotide overhang in the *URA3* gene. This reaction consisted of 80 μ L of pRS315URA3, 363 μ L water, 50 μ L of CutSmart buffer, and 7 μ L of NcoI restriction enzyme for a total of 500 μ L and incubated at 37 °C for 3-5 h. After at least 3 h, the digested plasmid was heated at 80 °C for 10 min to heat-inactivate the restriction

enzyme. The digestion was verified using a 0.7% agarose gel and the sample was stored at -20 °C. To obtain the DNA concentration, a Life Technologies Qubit 2.0 Fluorimeter was used following the manufacture protocol. Similar procedures were used in the digestion of pLKL67Y using the BmtI restriction enzyme in 1X 3.1 reaction buffer and pLKL103Y using BsmI and SacI restriction enzymes in CutSmart buffer with appropriate modifications in incubation temperature and heat inactivation temperature.

Nonhomologous end-joining DNA repair efficiency assays

The yeast mutant strains were transformed using NcoI-cut pRS315URA3 DNA to measure repair of 5' 4-nucleotide overhangs and BmtI-cut pLKL67Y DNA to measure repair of 3' 4-nucleotide overhangs, following the previously described early stationary phase and mid-log phase plasmid transformation protocols. Uncut pRS313 was used as a control for pRS315URA3 experiments to account for differing transformation efficiencies among the different mutant strains. Uncut pRS315 was used as the control for pLKL67Y experiments. Typically, each transformation consisted on 50-100 ng of digested plasmid DNA and uncut plasmid DNA. Each NHEJ assay included 3-4 independent replicates of each mutant strain, with 1 mL of cells put into each 1.5 mL microcentrifuge tube. BY4742 was used as wildtype control for NHEJ repair efficiency in *MAT α* strains, while BY4741 was used as the control for *MAT a* strains. Strains were inherently deficient in production of a nutrient required to grow on selective media (e.g. Leu⁻, His⁻, Ura⁻) and were only able to rectify this through uptake and repair of the plasmid DNA. For assessing NHEJ repair efficiency of 5' overhangs, cells were simultaneously transformed using pRS313 and NcoI-cut pRS315URA3. Successful uptake of pRS313 resulted in His⁺ colonies, and cells that took up and recircularized the

NcoI-cut pRS315URA3 became Leu⁺. Accurate repair resulted in Leu⁺Ura⁺ colonies. Repair efficiency was calculated by spreading transformant cells onto glucose minus leucine (Glu-Leu) and minus histidine (Glu-His) synthetic plates. Colonies able to grow on Glu-Leu plates represent successful recircularization of NcoI-cut pRS315URA3, and colonies that grew on Glu-His plates were successfully able to take up pRS313. To normalize transformation efficiency between mutant strains, the number of Leu⁺ transformants per µg of DNA was divided by the number of His⁺ transformants per µg of DNA.

This assay protocol was followed for all the other digested plasmids. For BmtI-cut pLKL67Y transformations, the *HIS3* gene was cut, and transformants were spread to Glu-Ura plates and uncut pRS315 was used as a control for transformation efficiency and spread to Glu-Leu plates.

Nonhomologous end-joining accuracy assays

To quantify the accuracy of the NHEJ repair, colonies forming on Glu-Leu plates (containing recircularized NcoI-cut pRS315URA3) were simultaneously patched onto fresh Glu-Leu and Glu-Ura plates using the same toothpick and grown at 30 °C for 2 days. Correctly repaired transformants were Leu⁺Ura⁺, while incorrect repair resulted in Leu⁺Ura⁻ cells. Leu⁺Ura⁺ cells had accurately repaired the DSB in the *URA3* gene from the NcoI digestion of the pRS315URA3 plasmid. A similar protocol was followed for assessing the accuracy with BmtI-cut pLKL67Y, where accurate repair of the DSB in the *HIS3* gene resulted in His⁺Ura⁺ able to grow on Glu-His and Glu-Ura plates. Each strain had greater than 100 colonies patched onto their respective plate for accuracy determination.

PCR addition and mutagenesis reactions

PCR was utilized in the creation of the pLKL103Y plasmid from pLKL91Y. The reaction mix used for this consisted of 10 μ M BsmJ (Phos-AGCATTCGAGCTCTCTTACTCTTGGCCTCCTCTAGTACA) primer, 10 μ M BsmK (Phos-AAAAGAAAATCCGGGAAAGGACTGTG) primer, a 1/10th dilution of pLKL91Y, 5X Phusion reaction buffer, 250 μ M dNTPs, and 1.6 units Phusion DNA polymerase for a total volume of 50 μ L. The reaction was completed in the Applied Biosystems 2720 Thermal Cycler with the following conditions for 34 cycles: 94 °C for 2 min, 56 °C for 30 s, 72 °C for 3 min 15 s. After completion of the cycles, the samples were held at 72 °C for 7 min, then stored at 4 °C. A similar reaction was used in the creation of pLKL104Y, the only alteration being the usage of the Leu2m1 (Phos-GCCGGCATCAGAACTGGTGATTTAGGTGGTTC) and Leu2m2 (Phos-ATCCAAAACCTTTTTAACTGCATC) primers in the reaction mix.

Construction of pLKL103Y plasmid

pLKL103Y was derived from the pLKL91Y plasmid via PCR addition of second BsmI and SacI restriction enzyme sites. This PCR reaction utilized primers created to ensure that the BsmI site was created within the plasmid's region of homology with the yeast chromosomal DNA, and the additional SacI site would provide further confirmation of the correct insertion location of the restriction enzyme sites. The primers also included a phosphate on the 5' end to allow for ligation and amplification via *E. coli* plasmid minipreps as described previously. The ligation of the plasmid was performed by using a reaction mix containing the PCR product DNA, 1X ligase buffer, and 400 units T4 DNA

ligase. This reaction mix was incubated at room temperature for 2h, followed by a heat inactivation of the T4 DNA ligase at 65 °C for 10 min, then placed on ice until the transformation began. After the transformation, 10 colonies were patched onto fresh LB + Amp plates then grown for 24 h. *E. coli* plasmid minipreps were performed on each of the ten patches and visualized on a 0.8% agarose gel. Successful minipreps were then digested with the SacI restriction enzyme and visualized with a 1.0% agarose gel. Those that displayed ~5,000 bp and ~1500 bp bands were tested again by digestion with BsmI. The plasmid digest was visualized on a 1.0% agarose gel, and the presence of a 500 bp band confirmed the correct addition of the restriction enzyme sites.

Nonhomologous end-joining vs Homology Directed Repair assay

BY4742 was transformed with BsmI-cut pLKL103Y using the early stationary phase transformation protocol to compare the occurrence of repair via both nonhomologous end-joining and homology directed repair. When digested with the BsmI restriction enzyme, pLKL103Y was cut twice, resulting in 2 nucleotide overhangs at each 5' end and a gap in the *HIS3* gene. If repaired via NHEJ, the transformant cell recircularized the plasmid and became Leu⁺Ura⁻. Utilizing the HDR pathway resulted in a cell that used homology with the chromosomal *his3-ΔI* to repair the gap in the plasmid, and the cell became Leu⁺Ura⁺. Uncut pRS316 was used a control for verification of competency of the yeast cells. Three separate replicates containing 1 mL overnight cell culture were transformed with 100 ng of BsmI-cut pLKL103Y and 50 ng of uncut pRS316. Separate aliquots of 150 μL, 100 μL, and 50 μL were spread onto Glu-Leu plates and one aliquot of 20 μL was spread onto a Glu-Ura plate for each replicate.

Uptake of pRS316 resulted in Ura⁺ colony growth on the Glu-Ura plate and indicated successful transformation of the plasmids. Colonies growing on the Glu-Leu plate were able to recircularize the pLKL103Y plasmid. Determination of the pathway of choice was done by patching 100 colonies onto Glu-Leu and Glu-His plates simultaneously and incubating the plates at 30 °C. Cells that repaired the plasmid using NHEJ were able to grow on the Glu-Leu plates, but not on the Glu-His plates. Using HDR to repair the plasmid yielded colony growth on both Glu-Leu and Glu-His plates, signifying successful repair of the gap in the plasmid. The patches were then counted to provide a percentage of colonies that utilized NHEJ versus those that used HDR.

III. RESULTS AND DISCUSSION

The NHEJ assays used for this project employed plasmids with a single DSB induced by a restriction endonuclease. The broken DNA was then transformed into yeast cells and repair resulted in recircularization of the plasmid (Figure 3). The plasmids used in this assay do not contain homology with any of the 16 yeast chromosomes, so repair can only occur via NHEJ (Figure 4).

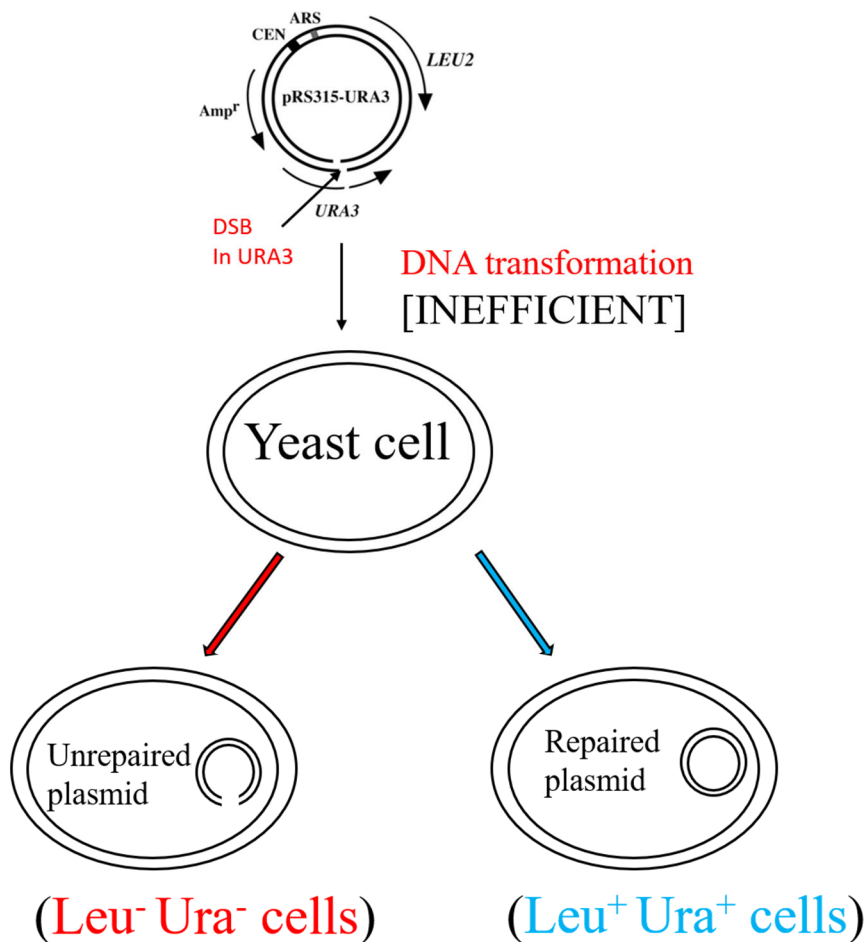


Figure 3. Transformation of plasmid DNA into yeast cells. Unrepaired plasmids do not imbue the phenotype for production of leucine and uracil (red arrow). Cells containing accurately repaired plasmids are able to grow on deficient media (blue arrow).

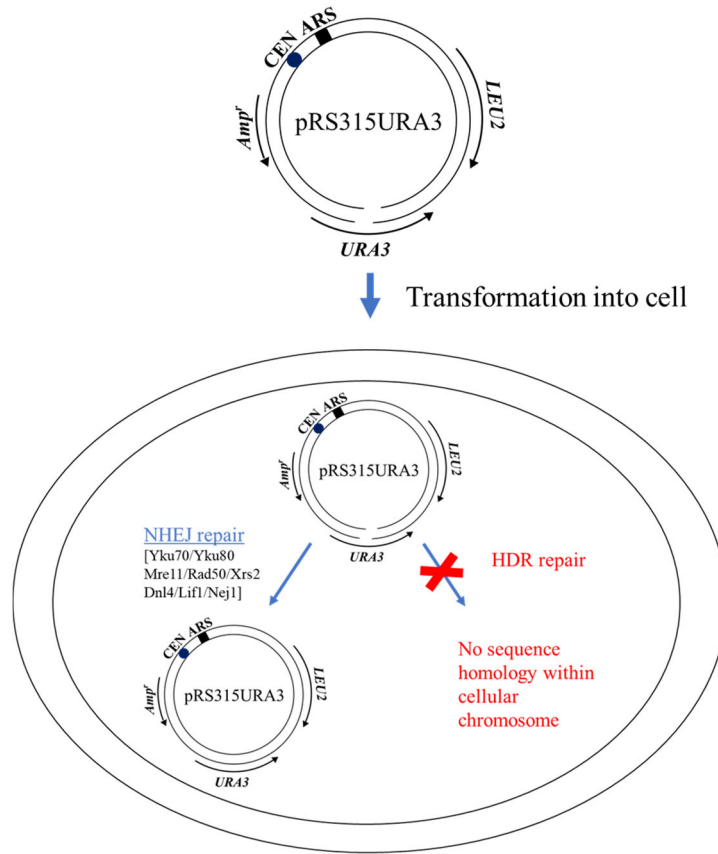


Figure 4. Diagram detailing plasmid repair pathways. Lack of sequence homology between chromosomal and plasmid DNA necessitates NHEJ repair.

Initial NHEJ assays were performed by introducing NcoI-cut pRS315URA3 (containing *LEU2* and *URA3*) into yeast cells through the optimized chemical transformation protocol. The plasmids do not contain homology to DNA within the cell, inhibiting the homologous recombination pathway and ensuring that NHEJ is the pathway utilized. After transforming the cells, aliquots were spread onto selective plates that did not contain leucine, meaning that only transformant cells that had taken up the plasmid could grow on the media (Figure 5). As shown in the figure, the assay allows distinction to be made between repair efficiency (recircularization of the plasmid) and accuracy (whether a mutation was introduced during the rejoining of the broken ends).

Accurate repair restores the wildtype *URA3* gene and cells become Leu⁺Ura⁺, while inaccurate repair leads to cells that are Leu⁺Ura⁻ (Figure 5).

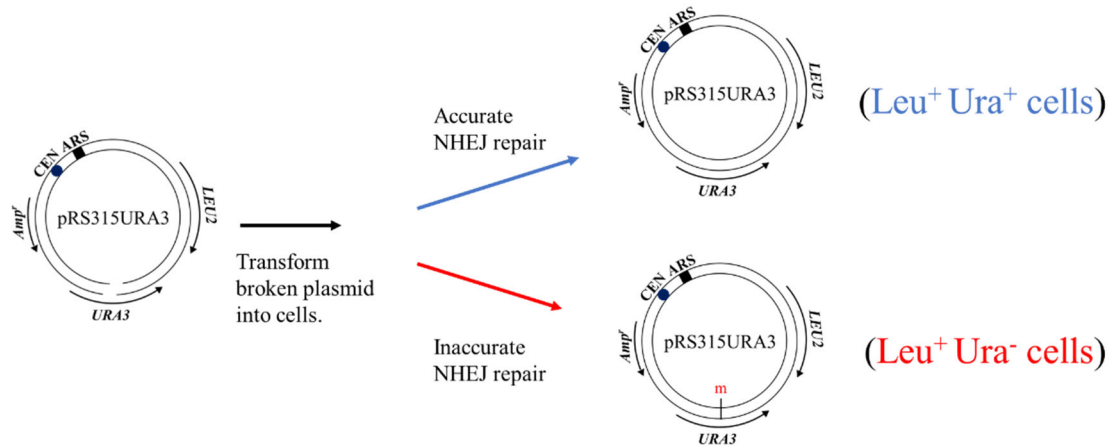


Figure 5. Diagram of NHEJ accuracy assays. Blue indicates accurate NHEJ repair, red indicates inaccurate repair resulting in inability to produce uracil. The lowercase “m” denotes a mutation in the *URA3* gene.

To accurately measure the NHEJ repair efficiency, uncut pRS313 plasmid was also transformed simultaneously with digested pRS315URA3 to normalize the results of the assay and account for general transformation efficiency of plasmids (Figure 6). To normalize the transformation efficiency, the ratio of Leu⁺ transformants to His⁺ transformants (NHEJ repaired pRS315URA3 plasmids/uncut pRS313 plasmids) is calculated as the DNA repair efficiency. The ratio of wildtype to *dnl4* repair efficiencies is calculated to determine the reduction in repair efficiency.

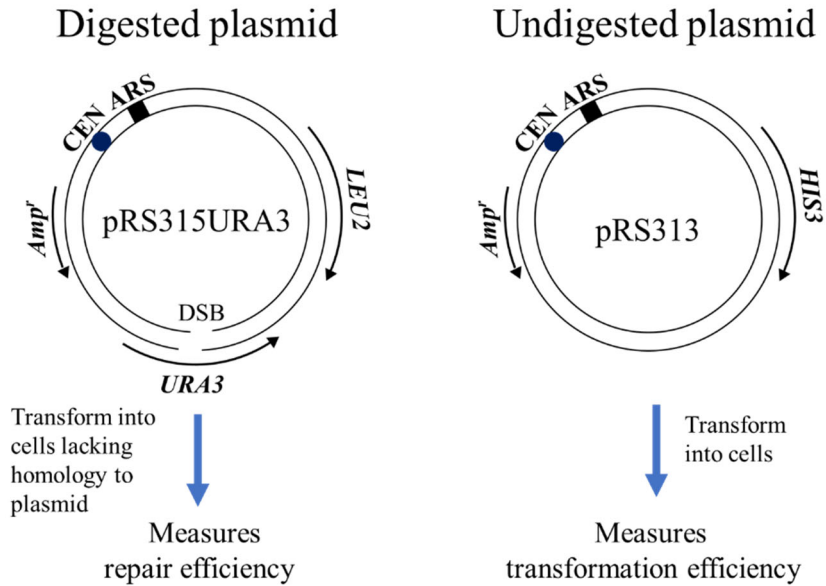


Figure 6. Normalizing of plasmid transformation efficiency vs repair efficiency.

Major goals of this project were to investigate the requirement for the three major protein complexes (Yku70-80, Mrx, and DNA Ligase IV) that mediate the NHEJ DSB repair pathway utilizing plasmid-based assays developed in the Lewis laboratory. To accomplish these goals, the Tripp *et al.* transformation protocol was optimized to increase the transformation efficiency of the plasmid assay and increase the number of transformant colonies⁴⁷. The protocol used in the experiments is shown on the left side of Figure 7. Cells were mixed with plasmid DNA and nonspecific carrier DNA (salmon DNA), followed by incubation with several chemicals that promote association of the plasmid DNA with the cells and uptake. The 42 °C heat shock step further promoted disorganization of the cell surfaces so that DNA could enter the cells. Two of the variables tested are shown in green text in Figure 7, and include the size of the salmon carrier DNA and the concentration of DMSO used to destabilize the cell wall and cell envelope.

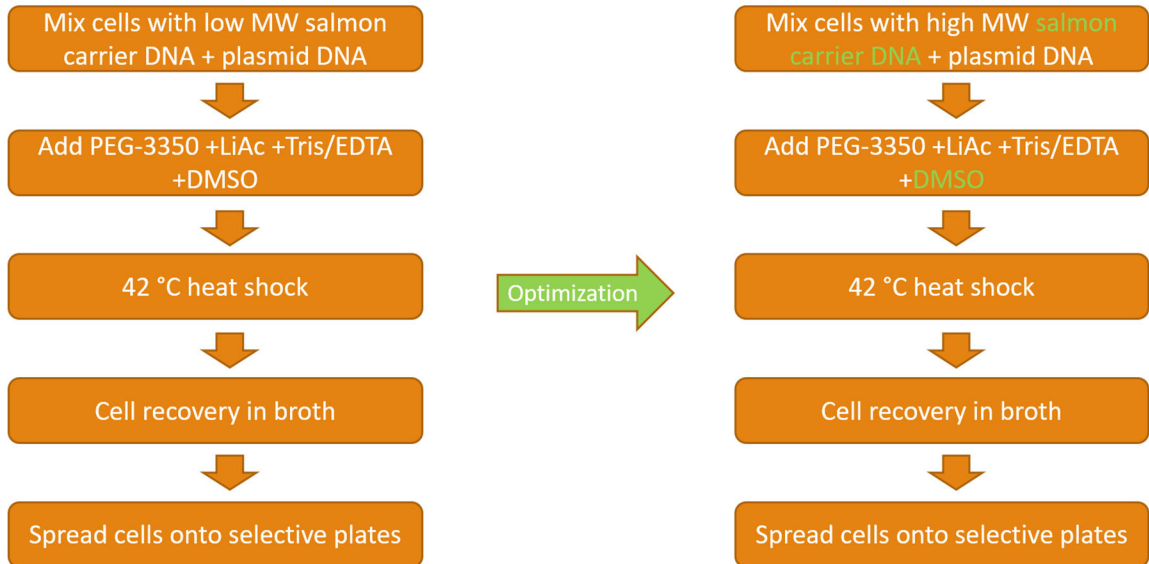


Figure 7. Comparison of unmodified and modified transformation protocol. Optimization of salmon carrier DNA and DMSO concentration improved yeast transformation. Green text indicates the optimization of specific components.

The transformation efficiency was increased two orders of magnitude by optimizing the sonicated salmon carrier DNA to have a higher molecular weight, specifically in comparison to the initial experiments using a low molecular weight version of the carrier DNA (Figure 8A, lanes 1 and 2 versus lanes 3 and 4). The ideal molecular weight for the carrier DNA was found to be an average of several thousand bp, instead of less than 500 bp that was previously used (Figure 8B).

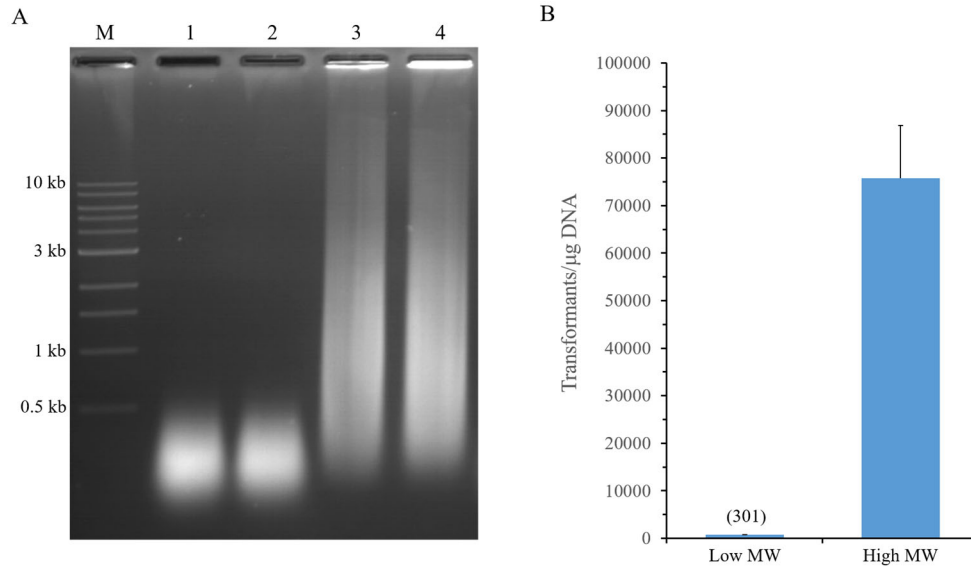


Figure 8. Comparison of transformation efficiency when using low or high molecular weight carrier DNA. (A) The initial salmon DNA used for transformation experiments had a MW of less than 500 bp (lanes 1 and 2); a new batch was acquired that had an average size of several thousand bp (lanes 3 and 4). The DNAs in each lane were aliquoted from different stock tubes. (B) The number of transformants was improved when using the higher MW salmon carrier DNA.

The second variable that noticeably impacted the transformation efficiency was the adjustment of the concentration of the DMSO. The optimal concentration was found to be 10-15%, which suitably disrupted the cell surface enough to allow passage of the plasmid DNA but did not terminally lyse the cell (Figure 9). All subsequent transformation experiments used 10% DMSO. Other variables investigated that did not notably increase transformation efficiencies included the cell incubation conditions, the final cell resuspension solution, and comparing older stocks of PEG-3350, DMSO, and LiAc to recently purchased stocks.

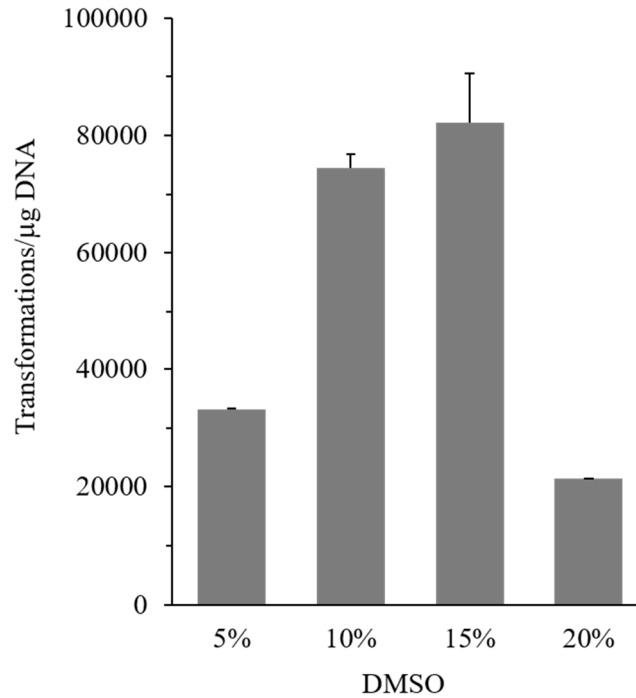


Figure 9. Comparison of transformation efficiencies using different DMSO concentrations. The optimal concentration for DMSO was determined to be 10-15%.

After improving the transformation efficiency, the second goal of the project was to evaluate the roles of the Yku, Mrx, and Dnl4 complexes in different cell cycle phases. The new, optimized protocol was used to perform NHEJ assays with NcoI-cut pRS315URA3 as shown in Figure 4. The results of the first two trials showed a 25-fold reduction of repair efficiency in DNA ligase IV-deficient *dnl4* mutants, in comparison to wildtype cells, which is consistent with previous results in the lab (Figure 10).

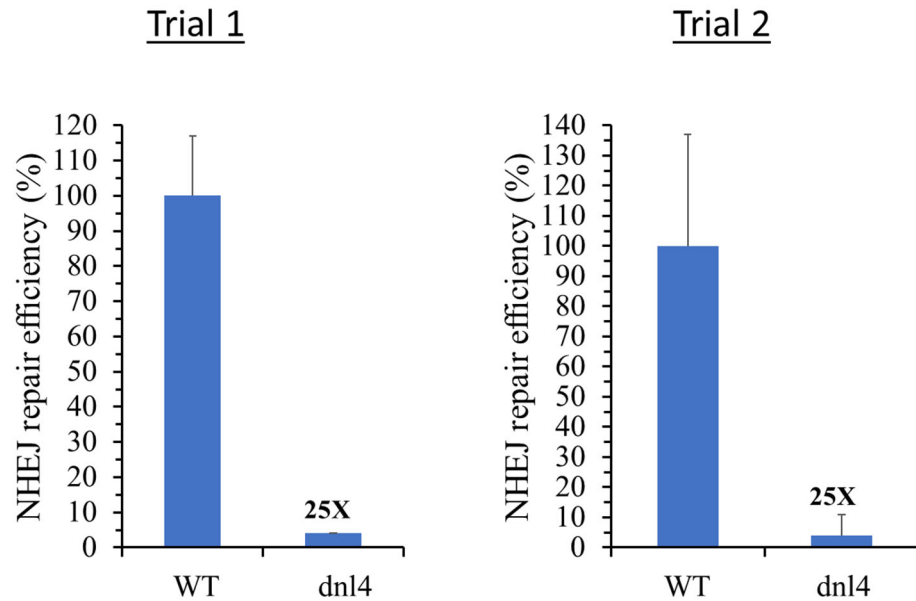


Figure 10. NHEJ repair efficiency of wildtype cells compared to *dnl4* mutants. The *dnl4* mutant showed a 25-fold reduction in NHEJ repair efficiency cells in two independent experiments.

This result with the *dnl4* mutant allowed work to move forward in expanding upon the results of previous graduate student Nestor Rodriguez by assessing the roles of the NHEJ complexes⁴². These new experiments would also compare the NHEJ repair assay results in the two different yeast mating types, *MAT α* and *MATa* cells, to verify if the differential Mrx complex requirement phenomena were consistent. Another goal of this project was to examine the role that cellular growth phase plays in NHEJ repair of DSBs. This was done by using the plasmid transformation assay to analyze the effect of the absence of each major protein complex involved in NHEJ during early stationary and mid-log phase cellular growth. Each variant of the plasmid transformation repair assay used the optimized protocol to transform plasmid digested using a restriction enzyme to

produce a DSB in a gene acting as a selectable marker along with an undigested plasmid as a control for transformation efficiency.

As described above, the preliminary NHEJ assays utilized the plasmid pRS315URA3 (Figure 11A). This plasmid contained the yeast *LEU2* and *URA3* genes as selectable markers, a centromere, and an origin of replication (ARS). For measuring NHEJ repair, pRS315URA3 was digested with the restriction enzyme *NcoI*, resulting in a DSB with 5' 4 nucleotide overhangs (Figure 11B). The pRS313 plasmid, in addition to a centromere and ARS, had the *HIS3* gene as a selectable marker to allow for separate analysis of the efficiency of the plasmid uptake in a particular cell strain.

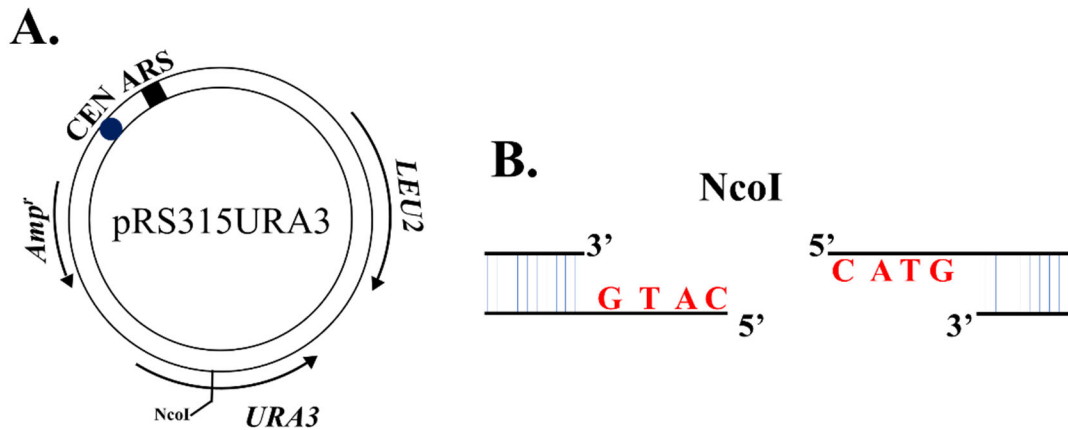


Figure 11. Diagram of pRS315URA3 plasmid. (A) The plasmid selectable markers are the *LEU2* and *URA3* genes and it contains an *NcoI* restriction site in the *URA3* gene. (B) Digestion with *NcoI* results in a single DSB with 5' 4 nucleotide overhangs.

This digestion was verified using agarose gel electrophoresis as shown in Figure 12. The gel compares the size of the uncut pRS315URA3 plasmid in lane 2 and the *NcoI*-cut linear form in lane 3.

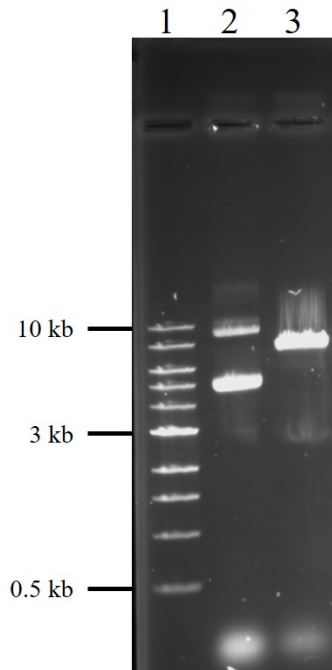


Figure 12. A 0.8% agarose gel electrophoresis showing *NcoI* digestion of the pRS315URA3 plasmid. Lane 1, 1 kb DNA ladder; Lane 2, Uncut pRS315URA3; Lane 3, *NcoI*-cut pRS315URA3.

The initial step of NHEJ is the binding of the heterodimeric Yku complex to protect the damaged DNA ends from degradation by nuclease activity. This step is in a dynamic competition with the Mrx complex, which has nuclease activity that could lead to a resection that does not allow for NHEJ to continue^{16,26}. After the initial commitment step to NHEJ, Mrx binds to Yku to tether the broken DNA ends to keep them in close proximity for the ligation step that is performed by the DNA Ligase IV complex. DNA Ligase IV aligns the two DNA termini to allow for the covalent joining of the broken strands^{16,32}. NHEJ repair is primarily utilized to repair DSBs in the G₁ cell cycle phase in yeast, while HDR is used predominantly in the other cell cycle phases³⁴.

For determining the requirement for each protein complex, one gene representing each protein complex was evaluated for its effect on efficient DSB repair. The absence of

the Yku70-80 complex was represented by the *YKU70* gene knockout, Mrx by the *MRE11* gene knockout, and DNA Ligase IV by the *DNL4* gene knockout. The optimized NHEJ repair efficiency assays initially focused on elaborating on previous results found in the Lewis laboratory suggesting that the Mrx complex may have a situational requirement in NHEJ repair, as opposed to the Yku70-80 and DNA Ligase IV complexes that were always required⁴².

The first series of experiments involving pRS315URA3 sought to investigate the requirement for the Mrx complex and determine what effect the cell cycle growth phase would have in the different NHEJ repair mutants (*yku70*, *mre11*, *dnl4*). The chemical-based transformation utilized was modified as described above to facilitate plasmid uptake. The quantity of plasmid DNA transformed into the cell was 100 ng of NcoI-cut pRS315URA3 plasmid along with 100 ng of uncut pRS313. These amounts of plasmids were transformed into four replicate cell cultures of *MAT α* wildtype and mutant *S. cerevisiae* cell strains with inactivated *yku70*, *mre11*, or *dnl4* genes. This initial experiment measured the transformation and NHEJ repair efficiency and sought to compare the results to Nestor Rodriguez's findings. The results of the early stationary phase NHEJ assay are shown in Figure 13. The strong reductions of the *dnl4* and *yku70* mutants (21- and 35-fold) compared to the *mre11* mutant (only 3-fold) support previous results found in the Lewis lab indicating that the Mrx complex may play a more situationally dependent role in NHEJ compared to Yku and DNA ligase IV.

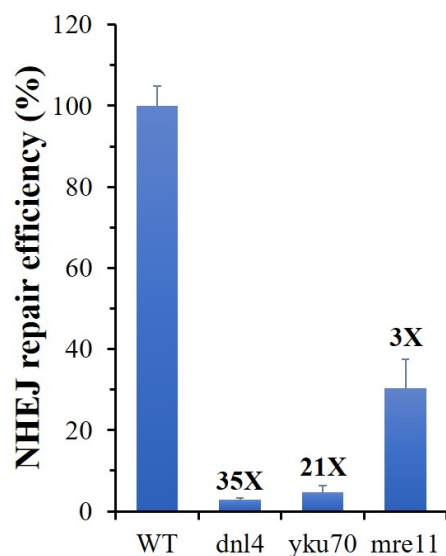


Figure 13. Different NHEJ repair complex requirements in early stationary *MAT α* *S. cerevisiae* cells. NHEJ repair efficiency was most reduced in *dnl4* and *yku70* strains. Each strain was tested using four cell cultures and the results were averaged. Bold numbers above the columns indicated fold reduction normalized to wildtype. Standard deviations are represented by the error bars in all graphs.

After each NHEJ repair efficiency assay was performed the accuracy of the repair was also determined. Although the NHEJ repair pathway is thought to be inherently more error prone than the HDR pathway, previous studies have detailed that the repair done by mutant cells with inactivated genes in NHEJ repair exacerbated the comparative lack of fidelity. The errors associated with NHEJ mutant strains were primarily small insertions/deletions (indels) located near the junctions of the repaired DNA ends^{16,20,39}. To determine the NHEJ repair accuracy, the plasmids used in this assay contain two genes that act as selectable markers, similarly to the NHEJ repair efficiency assay (Figure 5). As described above, the NcoI-cut pRS315URA3 plasmid contains a DSB in the coding region of the *URA3* gene, while the *LEU2* gene present on the plasmid is left intact (Figure 11). When repaired, the plasmid will always be Leu⁺ because

recircularization is required for the production of leucine. However, since the *URA3* gene has the DSB in the coding region, uracil production is dependent on accurate repair of the DSB, resulting in either Ura⁺ or Ura⁻ cells. Cells with plasmids that acquired a mutation in *URA3* would be able to grow on Glu-Leu (glucose minus leucine) plates, but due to the inability to produce uracil would be unable to grow on Glu-Ura plates. After transformation, cells were spread onto Glu-Leu plates, then Leu⁺ colonies were patched simultaneously onto Glu-Leu and Glu-Ura plates. The mutation frequency was calculated by dividing the number of Ura⁻ transformants by the total number of Leu⁺ transformants and normalizing to 100% for each strain tested.

The accuracy of NHEJ repair in the *yku70*, *dnl4*, *mre11* mutants displayed a similar trend to the repair efficiencies (Figure 14). The *dnl4* mutant was shown to have the highest mutation frequency among the three mutant strains tested at 94%, while the *yku70* mutant was the next highest at 72%, with the *mre11* mutant having the lowest at 0%. These results reinforce the idea that Mrx is not as critical for NHEJ repair of 5' overhangs as the Yku and Dnl4 complexes depending on the situation.

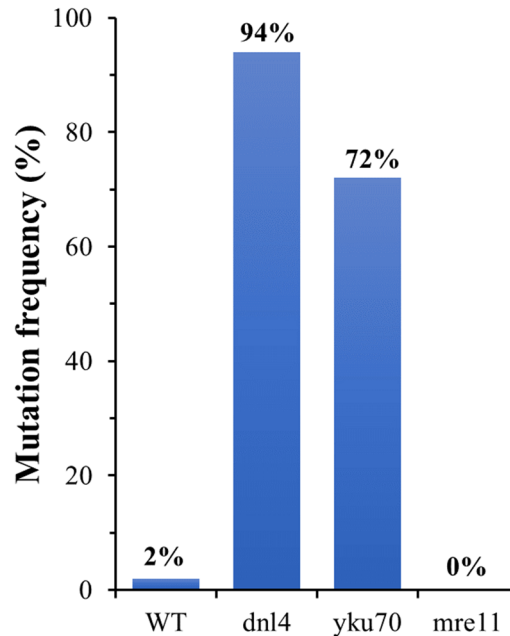


Figure 14. Early stationary phase NHEJ mutation frequency comparison of *MAT α* *dna14*, *yku70*, and *mre11* mutants. The mutants representing the Yku70-80 and DNA Ligase IV complexes are shown to have much higher mutation frequencies than wildtype and *mre11* cells. Numbers above the bars indicate the mutation frequency as a percentage.

As previously mentioned, in *S. cerevisiae* cells NHEJ is the primary pathway for DSB repair in G₁ due in part to the lack of a homologous template provided by sister chromatids available to utilize in HDR repair⁵⁰. Preliminary experiments conducted in the Lewis laboratory by Nestor Rodriguez suggested that cells in mid-log phase, unlike in early stationary and stationary phase cells, displayed an equal dependence on all three primary protein complexes⁴². His results are summarized in the figure below (Figure 15). He observed that each cell growth phase had a distinctive proportion of G₁ cells. The stationary and early stationary phases were shown to have high G₁ cell populations (90% and 60%, respectively) and did not absolutely require the Mrx complex for repair of 5'

overhangs. The necessity of the Mrx complex in log phase cells needed more investigation.

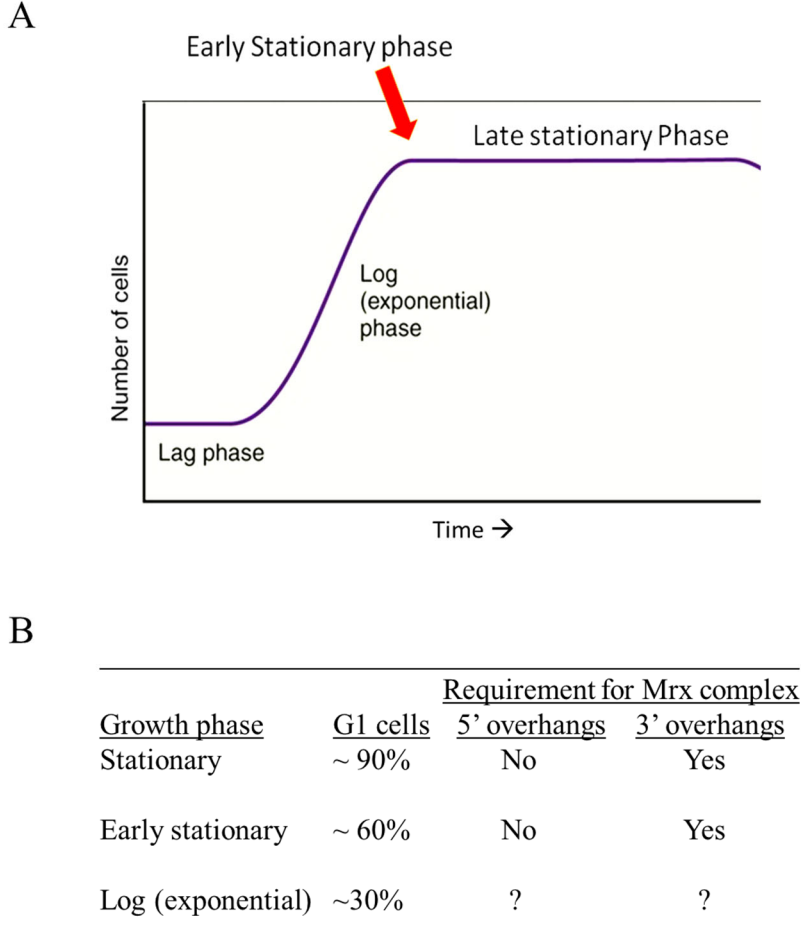


Figure 15. Percentage of G₁ cells in cell growth phases compared with requirement for Mrx complex in NHEJ repair. (A) Growth phases of cultured cells. (B) Percentage of G₁ cells in stationary, early stationary, and log growth phases. The requirement for the Mrx complex in NHEJ repair. Source of part A: <http://clinicalgate.com/bacteria-and-archaea/>

To further evaluate the role of cellular growth phase in the differential requirement for the Mrx complex, a log phase NHEJ repair efficiency assay was performed. The NcoI-cut pRS315URA3 plasmid was again used in combination with

uncut pRS313 to quantify the NHEJ repair efficiencies between the three different repair mutants. Unlike in the previous early stationary phase repair assay, in order to achieve mid-log phase growth, 3.0×10^6 cells per mL cultures were grown in separate 50 mL conical tubes that contained YPDA broth and were incubated for six hours. The rest of the transformation protocol and repair efficiency analysis was performed similarly to the early stationary phase assays.

In contrast to the results of the early stationary phase NHEJ assays, the requirements for each complex were relatively similar (Figure 16). The reduction for the *mre11* mutant (7.2-fold) was modestly higher than for the *yku70* and *dnl4* mutants (3.1-fold and 3.8-fold, respectively). This implied that there is a different requirement for the NHEJ repair complexes depending on the cellular growth phase.

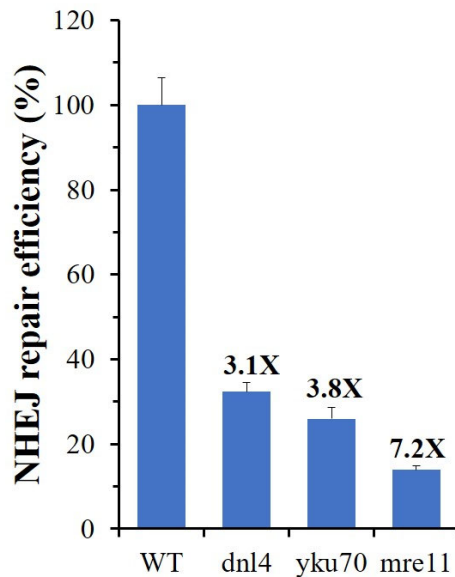


Figure 16. NHEJ repair efficiency for 5' overhangs in mid-log phase *MATα* cells. Reduction in NHEJ DSB repair efficiency is not as drastic in the mid-log phase *MATα* *dnl4* and *yku70* mutants compared to the early stationary phase repair assays. Importantly, Mre11 was at least as necessary for repair as Yku70 and Dnl4.

The mid-log phase accuracy tests were consistent with the results from the efficiency tests. In comparison to wild-type (5%) the *yku70* (62%), *mre11* (51%), and *dnl4* (58%) mutants displayed a greatly increased mutation frequency, indicating that all three repair complexes were necessary for efficient and accurate NHEJ repair in mid-log phase. Thus, each repair complex was shown to be similarly required for efficient NHEJ repair in mid-log phase and the mutation frequency was consistently increased in the absence of each of the repair complexes (Figure 17).

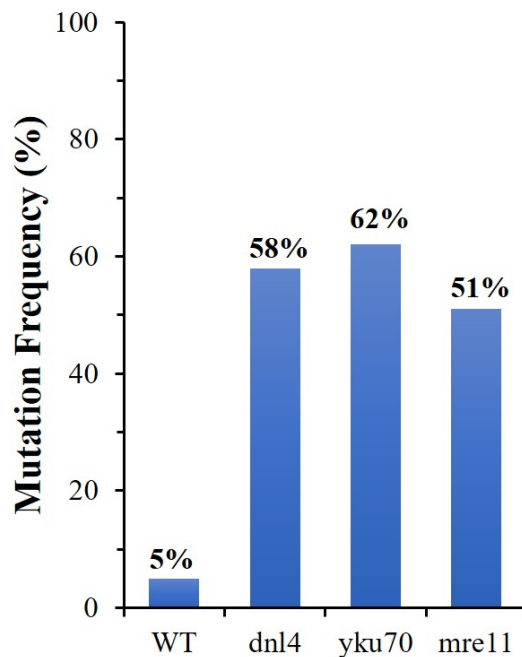


Figure 17. NHEJ mutation frequencies for 5' overhangs in mid-log phase *MATα* strains. The mutation frequencies in *dnl4*, *yku70*, and *mre11* mutants were similarly elevated.

The mating type of *S. cerevisiae* cells is determined by the presence of either the *MATα* or *MATa* mating locus on chromosome III⁵¹. MAT locus proteins, in conjunction with Mcm1, activate a set of genes specific to each mating type of the cell. We attempted to confirm that the results of the NHEJ assay using NcoI-cut pRS315URA in *MATα* cells

would give the same result in *MAT α* cells. The previous NHEJ efficiency assay was used to compare the requirement for the different NHEJ repair complexes in *MAT α* cells (Figure 18). These cells also showed a strong reduction in repair in *dnl4* and *yku70* mutants, but only a modest decrease in *mre11* mutants. Thus, the result was consistent between the two yeast mating types. These results indicate that this phenomena of the Mrx complex not playing as large a role in certain NHEJ repair situations is not restrained to a specific yeast mating type.

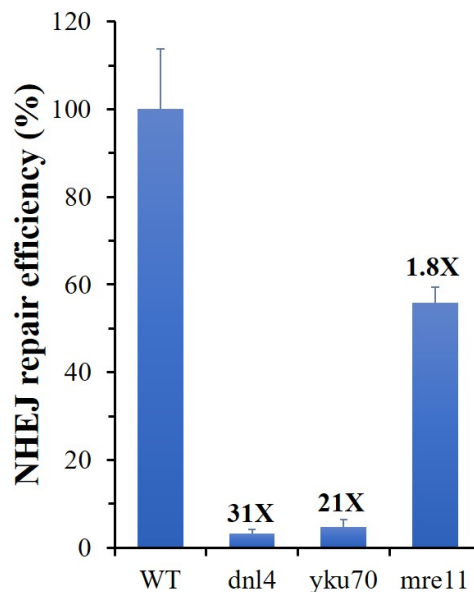


Figure 18. NHEJ repair efficiency of *NcoI*-cut pRS315URA3 in early stationary *MAT α* cells. NHEJ repair efficiency in the *dnl4*, *yku70*, and *mre11* mutant strains showed similar reductions in efficiencies to those in their *MAT α* counterparts.

Tests for NHEJ accuracy using *MAT α* cells in early stationary phase produced similar results to those found when using *MAT α* cells (Figure 19). There were very high mutation frequencies for the *yku70* and *dnl4* mutants, but not *mre11* cells. This result

indicates that both *MAT α* and *MATa* cells have a similar situational need for the Mrx complex and a consistent requirement for functional Yku and Dnl4 complexes.

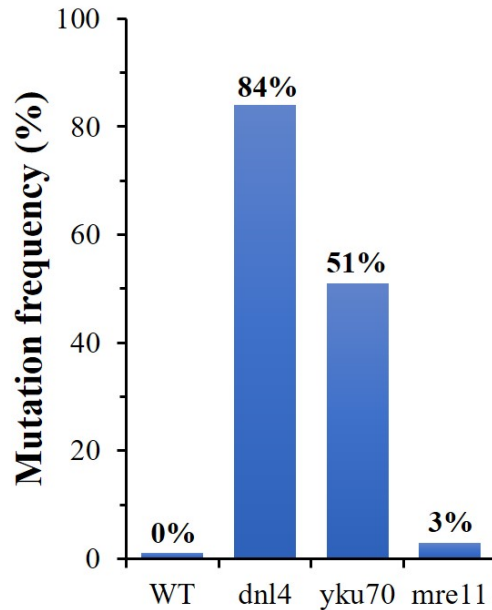


Figure 19. NHEJ mutation frequency in early stationary *MATa* cells. Mutation frequencies of the mutant strains were similar to those found in the *MAT α* cells, as the *dnl4* and *yku70* mutants had much greater mutation frequencies than the *mre11* mutants.

We analyzed NHEJ repair efficiencies in cells of the opposite mating type during log phase growth next. The previous assays using NcoI-cut pRS315URA3 and uncut pRS313 plasmids were repeated for *MATa* yeast cells. The log phase *MATa* cells exhibited equal requirements for the three primary NHEJ repair complexes (Figure 20). All three repair complexes showed comparable reductions, with *dnl4* (5.5-fold) and *yku70* (7.5-fold) being slightly less affected than *mre11* cells (8.6-fold). This result is consistent with the trend seen with the log phase *MAT α* cells (Figure 16).

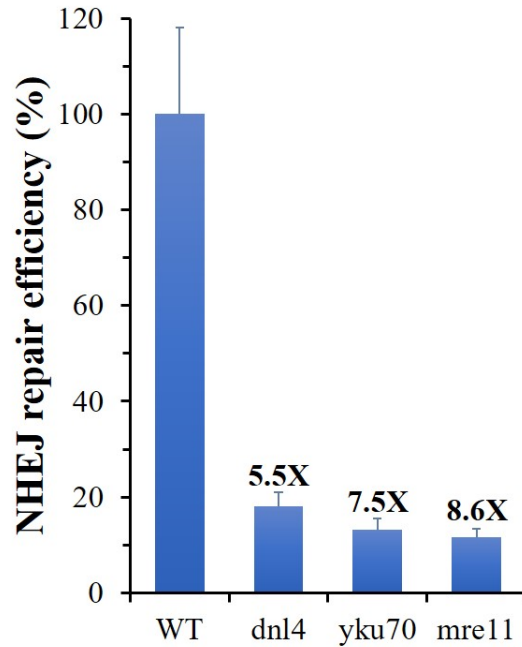


Figure 20. NHEJ repair efficiencies for 5' overhangs in mid-log phase *MATa* *dnl4*, *yku70*, and *mre11* mutants. The reductions are comparable with results from *MATα* cells.

NHEJ accuracy tests were used to quantify the mutation frequencies associated with loss of the primary NHEJ repair complexes in mid-log phase *MATa* cells. As before, mutation frequencies were high in all three mutants (Figure 21). However, the wild-type strain was shown to have an increased mutation frequency from what was expected (11%). Due to the modestly elevated mutation frequency in the wildtype strain, it is likely that this experiment should be repeated. The overall trend of high mutation frequencies in all three mutants in log phase is consistent with the log phase *MATα* cell experiments, however (compare Figure 17 to Figure 21).

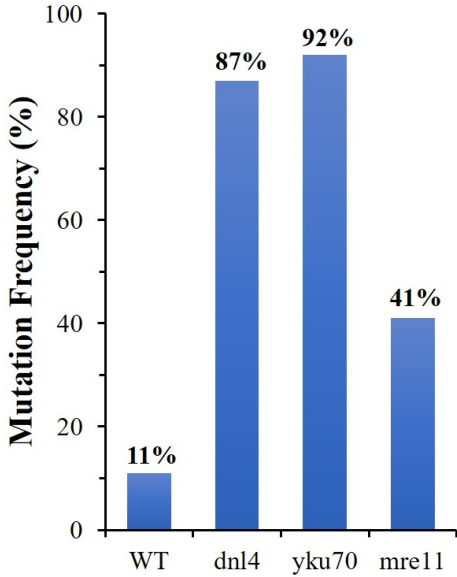


Figure 21. NHEJ mutation frequencies for mid-log phase *MATa dnl4*, *yku70*, and *mre11* mutants. Mutation frequencies are greatly elevated in log phase *dnl4*, *yku70*, and *mre11* mutants. The results are similar to those seen with log phase *MATα* cells.

NHEJ is the dominant pathway in G₁ phase in yeast, while HR is dominant in the other phases. Approximately 60% of cells in early stationary phase are in G₁, contrasting with the ~30% G₁ found in mid-log phase wildtype cells⁴². Since each cellular growth phase has a different composition of cells in G₁, this factor was hypothesized to play a role in the requirements for Mrx. To begin investigation of the different phases' effects on NHEJ mediation, the cells were to be arrested in G₁ phase using α-factor and in G₂ with the chemical nocodazole. α-factor is a pheromone secreted by *MATα* haploid yeast cells that can be purchased commercially. In the presence of α-factor, *MATa* cells will become arrested in G₁ phase.

The ability of α-factor to arrest *MATa* haploid yeast cells in G₁ phase was tested. This was attempted by using a 1/20th diluted overnight yeast culture of *MATa* wildtype

cells incubated in successively increasing concentrations of α -factor for two hours. The cells were visualized via phase-contrast microscopy to count the fraction of unbudded cells (signifying G₁ phase) and budded cells. Successful arrest would cause greater than 95% of cells to become unbudded G₁ cells. Initial results showed that only 61% of the cells were unbudded at the highest concentration of α -factor used (Figure 22). It was concluded that it was unlikely that a longer duration in α -factor would achieve a high enough percentage of G₁ cells, so follow-up experiments were designed to use higher concentrations of α -factor. This experiment could not be completed because of the pandemic lockdown. Future work will complete these experiments and also assess NHEJ repair in G₂ phase to determine if there is a differential requirement for the primary NHEJ complexes using nocodazole. Nocodazole is an inhibitor of microtubule polymerization, which is necessary for aligning the DNA in metaphase during mitosis. The drug causes activation of a cell cycle checkpoint that arrests the cell in G₂.

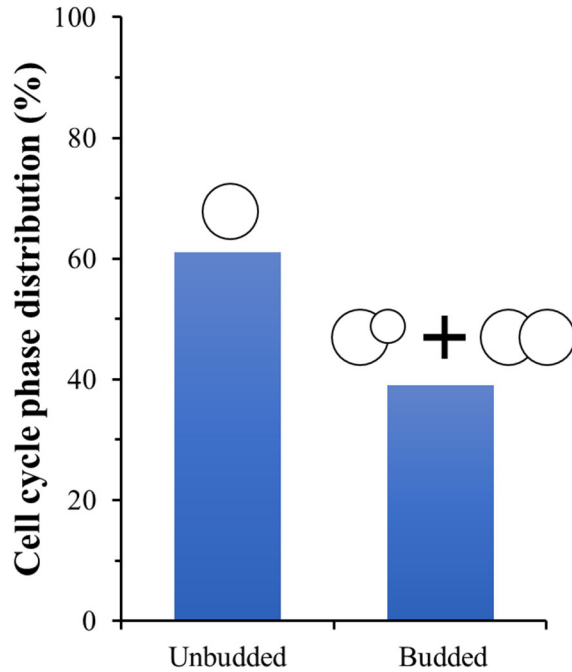


Figure 22. Percentage of unbudded (G₁) vs budded (S + G₂/M) cells. Unbudded cells are in G₁ phase, cells with a small bud are in S phase, and large-budded cells signify G₂/M phases.

The next set of experiments were performed to compare repair of DSBs with 5' ssDNA overhangs to those that have 3' ssDNA overhangs. The 3' hydroxyl group-containing ssDNA end is a preferred substrate of the Sgs1/Dna2 and Exo1 nucleases mediating the DNA resection step in the HDR repair pathway, which is in direct competition with NHEJ for repair of DSBs^{16,52}. This DNA resection is the commitment step of the HDR pathway that prevents NHEJ from occurring^{12,40}. The plasmid pLKL67Y was used in the next experiments (Figure 23A). This plasmid consists of the *URA3* and *HIS3* genes as selectable markers, a centromere, and an ARS. To induce a DSB containing a 3' overhang 4 nucleotides in length in the *HIS3* gene, the pLKL67Y plasmid was digested using the BmtI restriction enzyme (Figure 23B).

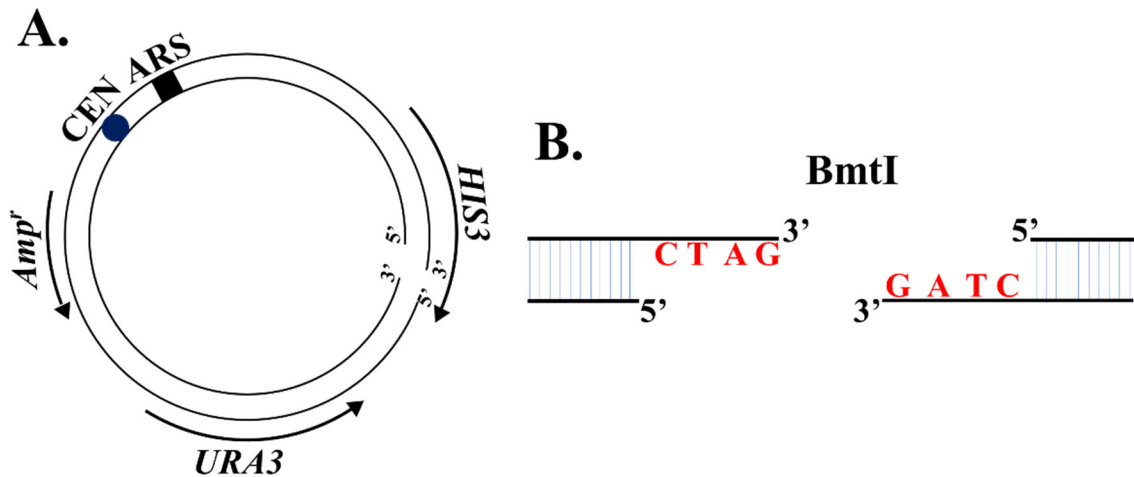


Figure 23. pLKL67Y plasmid diagram. (A) pLKL67Y plasmid showing a BmtI site in the *HIS3* gene. (B) BmtI DSB 3' overhang structure.

The NHEJ repair efficiency assays were performed using the same protocol as the previous early stationary phase efficiency assays, with the only change being the uncut plasmid used for the transformation efficiency control was pRS315 (*LEU2* selectable marker). The *yku70* (6.2-fold), *mre11* (6.4-fold), and *dnl4* (8.6-fold) mutants each displayed comparable reductions (Figure 24). This implies that each repair complex is equally important for efficient NHEJ repair of DSBs that contain 3' overhangs and supports the notion that the necessity for the Mrx complex may be dependent on end structures.

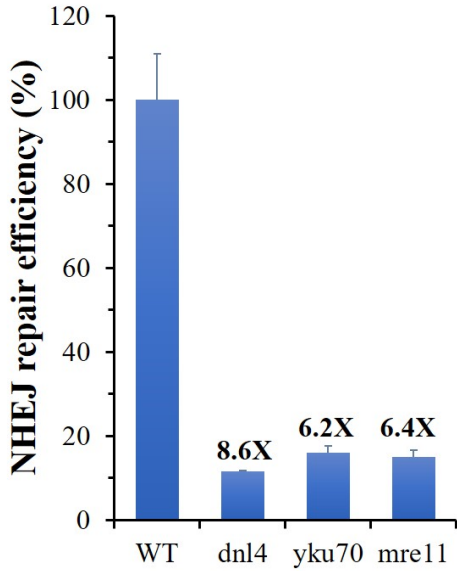


Figure 24. NHEJ efficiency assay using BmtI-digested pLKL67Y in early stationary phase *MAT α dnl4, yku70, and mre11* mutants. Each mutant strain has similarly reduced repair efficiency.

Mutation frequencies were high in all three mutants when DSBs with 3' overhangs were tested in early stationary phase cells. The *dnl4* and *yku70* mutants had the highest mutation frequencies at 86% and 74%, while the *mre11* mutant had the lowest frequency at 22% (Figure 25). These results show that the efficiencies of recircularization of the plasmid were very similar between the three repair mutants, but the accuracies of repair by NHEJ were not. Cells appeared to have more of a requirement for the Yku and DNA Ligase IV complexes than the Mrx complex for accurate repair of 3' overhangs in early stationary phase cells.

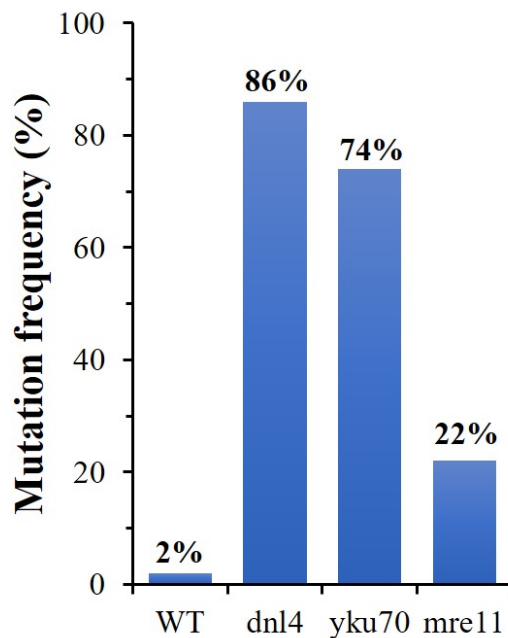


Figure 25. NHEJ mutation frequencies for 3' overhangs in early stationary phase *MATα* cells. The NHEJ mutation frequency was increased in all three mutants. The *mre11* mutant mutation frequency was not as elevated as *dnl4* and *yku70* despite similar NHEJ repair efficiencies for DSBs with 3' overhangs.

The NHEJ repair efficiencies of DSBs with 3' overhangs were analyzed next using mid-log phase cells. Similar to results with 5' overhangs, Mrx was needed for efficient repair during log phase. The primary difference was the stronger reduction in the *mre11* mutant (15.3-fold) compared to the *dnl4* (4.9-fold) and *yku70* (4.2-fold) mutants (Figure 26). This result provides evidence that the requirement for Mrx is dependent on both the cellular growth phase as well as the type of DNA end that needs to be repaired.

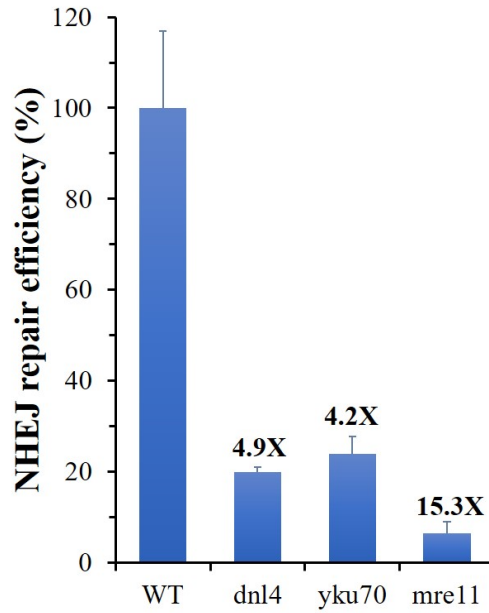


Figure 26. NHEJ repair efficiency of BmtI-digested pLKL67Y using mid-log phase *MAT α* cells. Repair efficiencies were reduced in all three mutants.

Analysis of repair accuracies for DSBs with 3' overhangs in log phase cells revealed that the mutation frequency was elevated to a similar degree for all the mutant strains in comparison to wild-type (Figure 27). These results differ from those with early stationary phase cells (Figure 25) where mutation rates were much higher in *yku70* and *dnl4* mutants than in *mre11* cells.

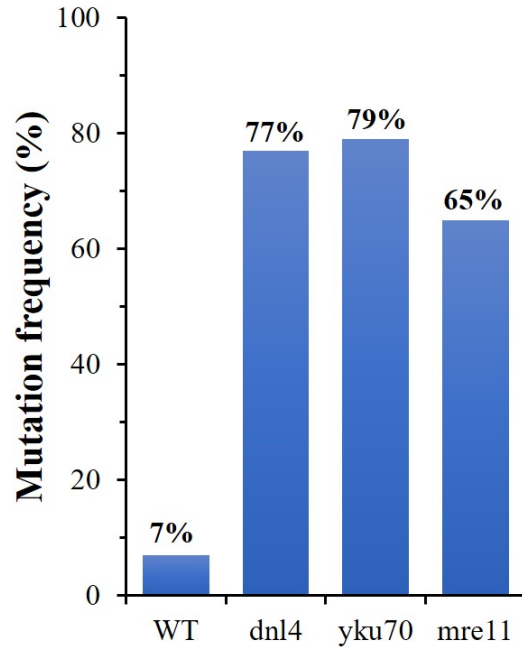


Figure 27. NHEJ repair mutation frequencies in mid-log phase cells using BmtI-digested pLKL67Y. The mutation frequency is consistently increased across the *dnl4*, *yku70*, and *mre11* mutant strains compared to wildtype.

In most NHEJ assays performed previously, 100 ng of cut plasmid DNA was used for each transformation. The possibility that the amount of DNA added to the cells might influence the results was tested. Three separate plasmid transformation assays using different amounts of digested plasmid DNA (100 ng, 25 ng, and 12.5 ng) and 50 ng of uncut plasmid were performed on wildtype and *dnl4* cell strains. The result was a consistent 40- to 60-fold reduction in the *dnl4* mutants (Figure 28A). This suggested that the amount of digested plasmid DNA had little effect on the reduction in repair seen in *dnl4* mutants.

The next experiment was designed to determine if the results showing that the Mrx complex was not as critical as Yku and Dnl4 was affected by the amount of DNA. This was done by performing assays with 25 ng of digested pRS315URA3 using *yku70*,

mre11, and *dnl4* strains and following the NHEJ early stationary phase protocol. The *yku70* and *dnl4* mutants exhibited 83- and 66-fold reductions, while *mre11* cells were only decreased by 4.7-fold (Figure 28B). This result is consistent with the previous tests of early stationary phase cells (Figures 13 and 18), indicating that the amount of DNA used was not a factor.

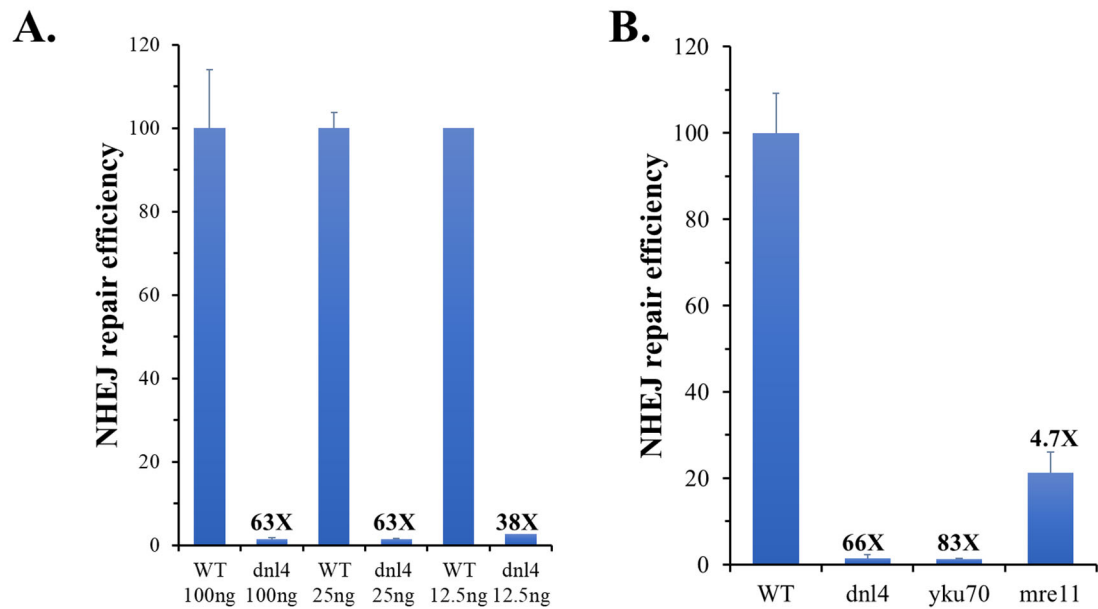


Figure 28. Repair efficiency reduction with different amounts of cut plasmid. (A) Comparison of repair efficiencies with wildtype and *dnl4* cells when 100 ng, 25 ng, and 12.5 ng digested plasmid is used for transformations. (B) Reduced requirement for Mre11 seen with 25 ng DNA is comparable to previous results using 100 ng DNA.

The next goal was to characterize new NHEJ mutants that could influence NHEJ repair efficiency and accuracy. Graduate student Jennifer Lilley performed a genomics screen of a yeast mutant library to identify new NHEJ repair mutants using a plasmid-based NHEJ assay⁴³. She identified 3 new genes that affected repair efficiency (*ARP5*, *BUD32*, and *MCT1*) in both *MATa* and *MATα* yeast strains (Figure 29). NHEJ repair accuracy was also shown to be reduced by inactivation of 3 other genes (*LSM7*,

RTF1, and *MCT1*). Experiments for the current project focused on the Arp5 protein in the INO80 complex that is involved in chromatin remodeling. These experiments also assessed the roles of Arp6 and Arp8, as they are nonessential proteins that are involved in the same complex. Work by Susan Gasser's lab suggested that Arp proteins may have a function in DNA repair, however the exact function is still unknown^{44,46}. It has been shown that chromatin remodeling plays a role in NHEJ repair efficiency (with the RSC complex), so the importance of Arp5 and other associated proteins in NHEJ were tested.

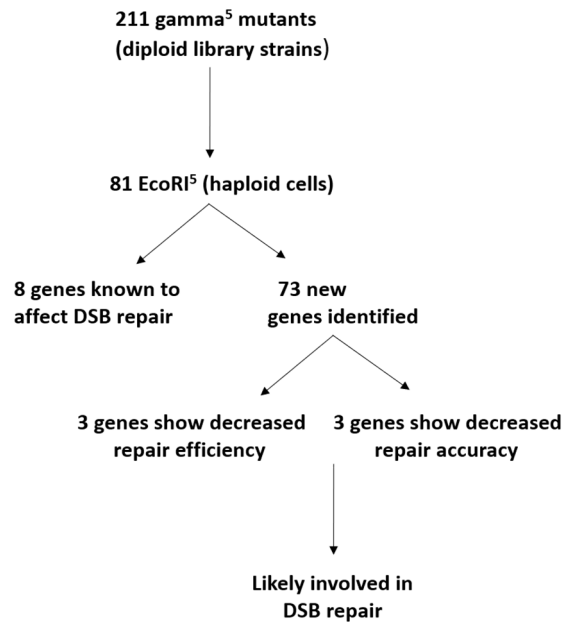


Figure 29. Genomics screen identified new NHEJ repair mutants⁴³.

To begin characterization of the chromatin remodeling proteins implicated in the genomics screen, the first experiment sought to reproduce the previous results from Jennifer Lilley involving Arp5⁴³. She observed that *arp5* mutants had a 6- to 8-fold reduction in NHEJ efficiency when tested using the early stationary phase plasmid transformation assay with NcoI-cut pRS315URA3. The experiment in this project used

wildtype, *dnl4*, and *arp5* yeast strains and followed the same transformation protocol as previously described, with the modification of using 25 ng of NcoI-cut pRS315URA3. The *dnl4* mutant strain acted as control to ensure that the results were consistent with previous NHEJ assay findings. In contrast with the reduction found by Jennifer Lilley, the *arp5* mutant strain tested in this project showed only a 1.1-fold reduction, indicating approximately wildtype efficiency (Figure 30A). The experiment was repeated to verify the reproducibility of this result. The same experimental protocol was followed in a second experiment and *arp5* only displayed a reduction of 1.3-fold (Figure 30B). These results imply that there may be an unknown technical difference between the *arp5* NHEJ repair experiments done in this project and those performed by Jennifer Lilley. The library mutants were not tested further.

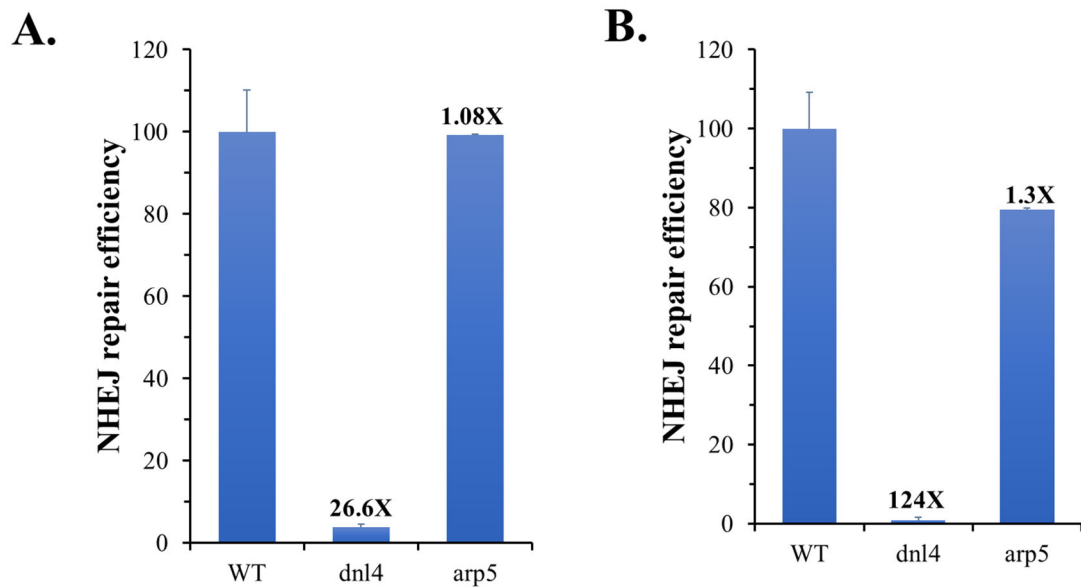


Figure 30. NHEJ repair efficiency of *arp5* cells. (A) First *arp5* NHEJ repair assay with wildtype and *dnl4* controls. (B) Repeated repair assay.

As previously mentioned, DSB repair pathway choice between NHEJ and HDR is primarily dictated by the DNA end resection completed by nuclease activity that initiates HDR^{16,53}. Repair pathway choice is further mediated by the presence of Rif1 or Nej1 proteins that may protect the DNA ends from resection and allow for the progression of NHEJ^{17,54}. We hypothesized that the determination of repair pathway choice could be tested more easily if a single plasmid could be used to test both pathways in the same experiment. Therefore, to explore the contributing factors of DSB repair pathway choice in yeast cells, a new plasmid was created, pLKL103Y. This plasmid was derived from the plasmid pLKL91Y and has the *HIS3* gene as a selectable marker (Figure 31). The pLKL103Y plasmid was created through the PCR addition of second BsmI and SacI restriction enzyme sites (in addition to those already in the pLKL91Y plasmid).

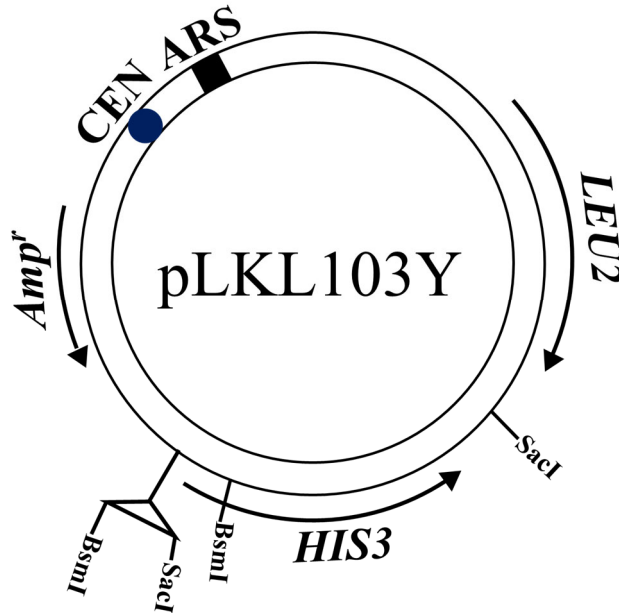


Figure 31. Diagram of new pLKL103Y plasmid. PCR addition of a second BsmI restriction enzyme site allows for the creation of a gap in the *HIS3* gene to be used as a selectable phenotype in NHEJ vs HDR DNA repair assay.

The second BsmI site was added in *HIS3* by PCR mutagenesis with primers bsmJ and bsmK so that upon digestion of the pLKL103Y plasmid with BsmI, the linearized plasmid would have a 433 bp gap in the *HIS3* gene (Figure 32). The additional SacI site was used for further confirmation of the accuracy of the PCR addition of the new BsmI site. pLKL103Y was verified using agarose gel electrophoresis to visualize the products of the plasmid when digested with SacI and BsmI (Figure 33). Since the full size of the plasmid was roughly 6500 bp, the SacI digest should have resulted in bands of approximately 5000 bp and 1500 bp as seen in lane 2. The BsmI digest products were expected to be approximately 6000 bp and 500 bp, which is shown in lane 3.

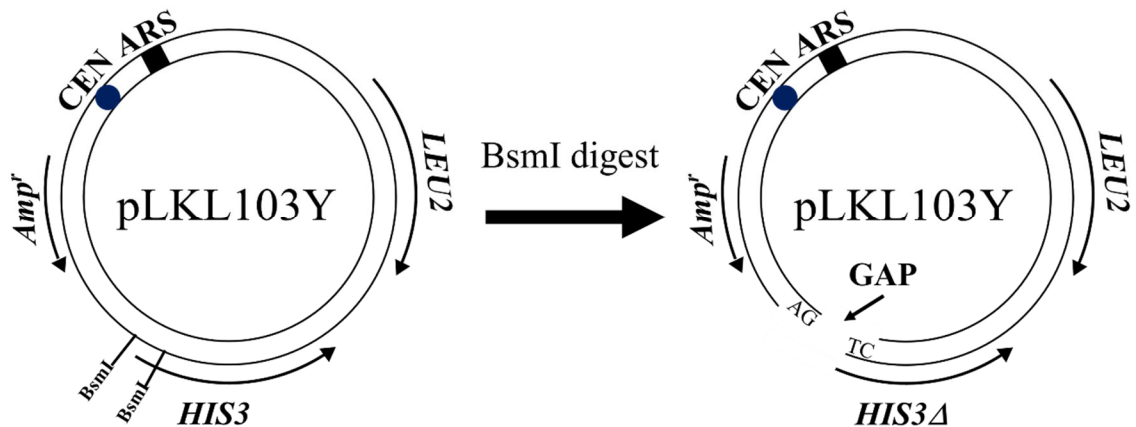


Figure 32. BsmI-digestion of pLKL103Y. Digestion at two BsmI restriction sites allows for creation of 433 bp gap in the *HIS3* gene. The resulting DNA end structure is a complementary 2 bp 5' overhang. This gap region has homology with the chromosomal *HIS3* gene and can only be fully repaired via homologous recombination between the plasmid and the chromosome.

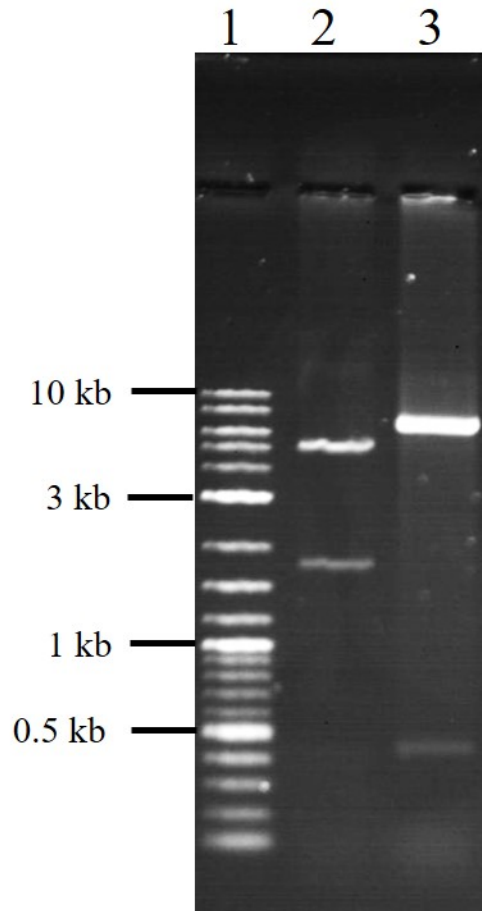


Figure 33. BsmI and SacI digestion of pLKL103Y visualized using 0.7% agarose gel electrophoresis. Lane 1, 2-log DNA ladder; Lane 2, SacI digest of pLKL103Y; Lane 3, BsmI digest of pLKL103Y.

The repair of gapped pLKL103Y produces different phenotypes depending on whether repair occurs by NHEJ or HDR. Repair by NHEJ simply ligates the broken ends together, resulting in a deletion in *HIS3* and cells that are Leu⁺ but His⁻ (Figure 34A, left side). Since the pLKL103Y *HIS3* gene contains homology with the chromosomal *his3-Δ1* gene, the HDR repair pathway could be used to accurately repair the plasmid *HIS3* gene too. If the gap in *HIS3* is repaired by homologous recombination using the chromosomal *his3-Δ1* gene as a template, the cells will become Leu⁺ and His⁺ (Figure 34A, right side).

The BsmI-digested pLKL103Y plasmid was transformed into wild-type *S. cerevisiae* cells using the new transformation protocol and grown for three days on synthetic Glu-Leu cell culture plates. The Leu⁺ transformants were then patched onto Glu-His plates to test whether the cells were Leu⁺His⁺ or Leu⁺His⁻. The results showed that NHEJ repair was used in 95% of the transformants (Figure 34B). The low frequency of repair by recombination was unexpected. It is likely that it occurred because there was only approximately 100 bp of homology with the chromosome on either side of the plasmid gap. The efficiency of recombination is reduced when levels of homology are decreased.

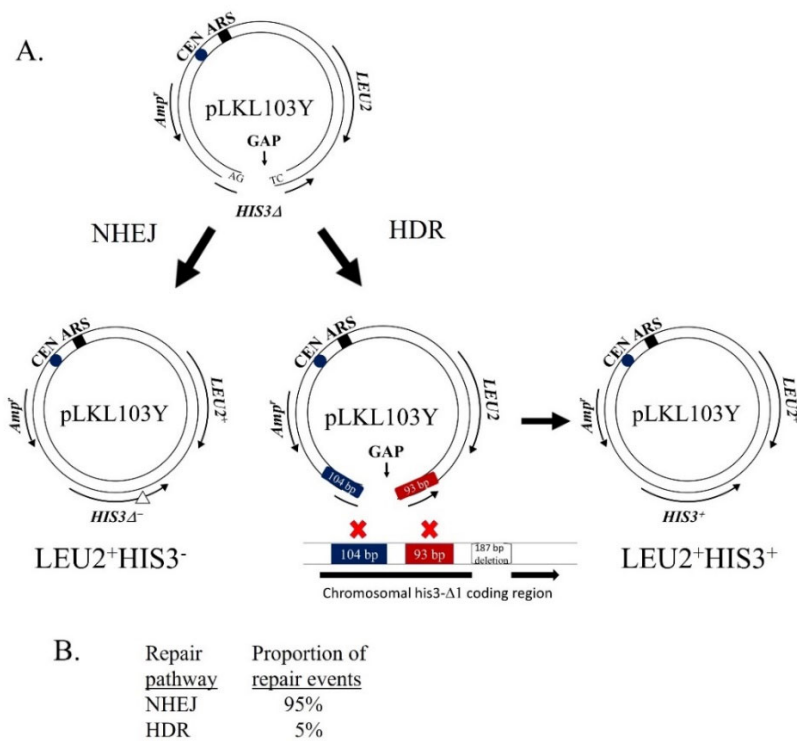


Figure 34. NHEJ vs HDR repair pathway choice using pLKL103Y. (A) pLKL103Y was digested with BsmI to produce a 433 bp gap in the plasmid. The DNA end structure around the gap contained complementary 2 nucleotide 5' overhangs. This gap was flanked by homologous regions so that either HDR or NHEJ could be utilized for repair. (B) Results of the repair assay showed that the predominant pathway choice was NHEJ, which produced Leu⁺His⁻ cells.

A new gapped plasmid system was designed to overcome the problems encountered with pLKL103Y. A new plasmid was created using PCR mutagenesis to eliminate the single BspMI site in pLKL91Y so that it would not interfere with digestion to produce a gap in the plasmid (Figure 35). The new plasmid, pLKL104Y, has two base-pair substitutions in *LEU2* that are silent. They destroy the BspMI site in the gene but do not alter the amino acid sequence of the protein (Figure 35, lower left). This new plasmid was created by ligation with T4 DNA ligase and transformation into *E. coli* cells to produce colonies on LB + ampicillin plates. Analysis of the plasmids in these colonies was delayed by the pandemic lockdown and will be completed in June and July.

sequence. Type IIS enzymes are different in that they bind to their target sequence and then make a DSB several base-pairs upstream or downstream of their recognition site. The Type IIS enzyme BspMI binds to its target sequence of ACCTGC and then cuts 4 nucleotides to the right on the upper strand and 8 nucleotides to the right on the lower strand. The digestion produces 5' ssDNA overhangs that are 4 bases long, where the cuts are shown by the up arrows shown in the small box labeled "BspMI digestion" in Figure 36A.

The new design involved amplifying the plasmid pLKL104Y by PCR primers that each have a Type IIS BspMI site in them. The primers are shown in Figure 36A as the small red arrows labeled with "IIS" on their ends. The primers anneal with the coding region of *HIS3* and prime in opposite directions, but do not amplify the whole plasmid. A gap is left between the priming sites. Following PCR amplification, the resulting fragments are digested with BspMI, which cuts internally within the *HIS3* coding region which is perfectly homologous with the coding sequences of the chromosomal *his3-Δ1* gene. A Type II enzyme could not be used for this PCR product because after the cleavage a portion of inserted, nonhomologous DNA sequence would remain on the ends, interfering with HDR. If the primers contained no restriction sites, a blunt ended product would be produced, which would inhibit NHEJ and have the 4-nucleotide complementary overhang the previous experiments contained.

In the first experiments using pLKL103Y, the gapped plasmid was created by cutting the DNA with BsmI, which cuts twice within the plasmid. In the new system, the PCR product that has been cut with BspMI on the ends represents the gapped plasmid transformed into the cells. This relationship is shown in Figure 36B, which demonstrates

how the PCR product can also be represented as a gapped circular plasmid. The PCR primers were designed to anneal in the middle of *HIS3* to amplify a fragment that has more homology to *his3-Δ1* on the ends than were present when pLKL103Y was used previously. Increasing the homology on each end from approximately 100 bp to 200 bp should increase homologous recombination efficiency and avoid having 95% of repair events utilize NHEJ as with the previous experiment.

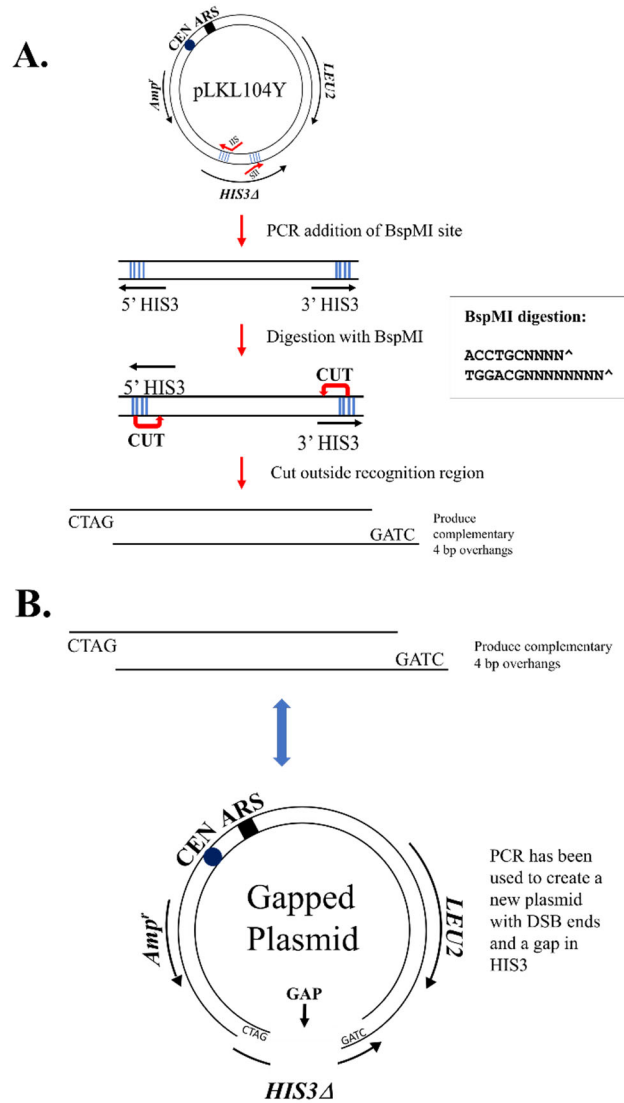


Figure 36. PCR addition of BspMI sites and digestion of plasmid to create gap in *HIS3* gene. (A) The addition of two BspMI restriction enzyme sites on the PCR-amplified pLKL104Y plasmid allows for the creation of a 207 bp gap in the *HIS3* gene. The BspMI Type IIS enzyme makes an incision outside of its recognition site for the creation of two complementary 4 nucleotide overhangs to be repaired via NHEJ or HDR. (B) The linearized, gapped plasmid can be transformed into *S. cerevisiae* cells for repair.

IV. SUMMARY AND CONCLUSIONS

The NHEJ repair pathway is mediated by the Yku, Mrx, and Dnl4 protein complexes. These complexes are encoded by eight genes: *YKU70*, *YKU80*, *MRE11*, *RAD50*, *XRS2*, *DNL4*, *LIF1*, and *NEJ1*. Each complex is thought to play an important role in the efficient and accurate repair of DSBs. Previous work in the Lewis laboratory suggested that there is a more situational requirement for the Mrx complex depending on the cellular growth phase and the DNA end structure that is being repaired (5' vs 3' overhangs)⁴². Plasmid transformation assays were used to quantify the effect of inactivated genes by measuring the efficiency and accuracy of the repair of DSBs via NHEJ. In order to ensure that the assays were accurately depicting the NHEJ repair in the mutant strains, the transformation protocol was also optimized. This study tested NHEJ repair efficiency and accuracy in early stationary phase and mid-log phase *yku70*, *mre11*, and *dnl4* mutant cells. In addition to this, the role of DNA end structure was also evaluated. A novel method of determining the DSB repair efficiency in both NHEJ and HDR in a single assay was also established in this project.

The NHEJ repair efficiency of the plasmids that contained a DSB with 4 nucleotide 5' overhangs was shown to be strongly decreased in early stationary phase *yku70* and *dnl4* cells, while repair in *mre11* cells was only modestly affected. This trend was maintained when assessing the accuracy of the repair, with the *yku70* and *dnl4* mutants showing much higher mutation frequencies than the *mre11* mutant. The results of the repair and accuracy assays indicated that there was less of a requirement for the Mrx complex than the Yku and Dnl4 complexes when the cells were in early stationary

phase. NHEJ assays using the same plasmid in mid-log phase cells indicated that all three repair mutants displayed similar decreases in repair efficiency. The early stationary and mid-log phase repair and accuracy experiments were repeated in *MATa* cells and they yielded similar results. One of the major differences between early stationary phase and the mid-log phase cells is the higher percentage of G₁ phase cells in early stationary phase (Figure 37)⁴². In order to assess the role of the higher G₁ cell composition, an α -factor experiment was attempted. This was unsuccessful due to an inability to obtain a high enough percentage of G₁ phase cells, so this experiment will be attempted later this summer using a higher concentration of α -factor.

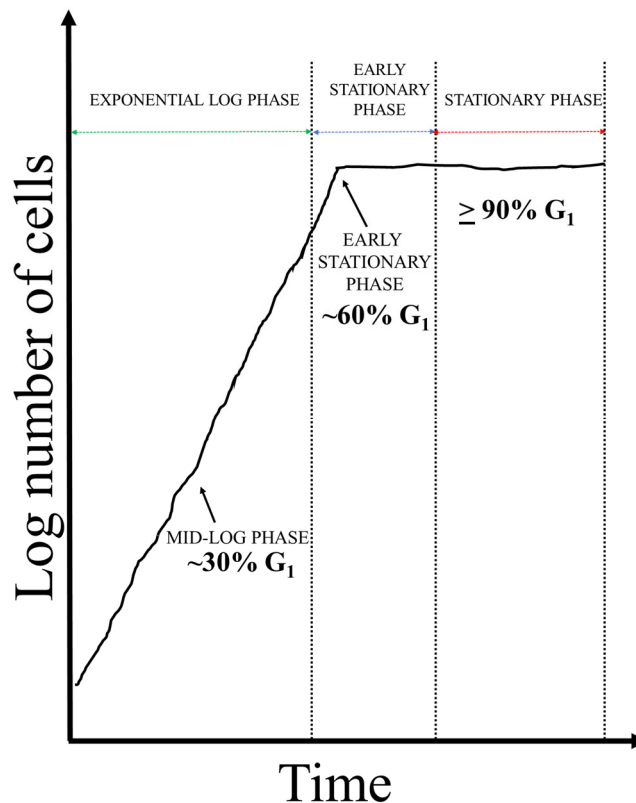


Figure 37. Diagram of cellular growth phases. Early stationary (~60%), stationary ($\geq 90\%$), and mid-log (~30%) phase have different distribution of cells in G₁ phase.

The next NHEJ experiments investigated repair of DSBs containing 3' ssDNA overhangs. Repair efficiencies of BmtI-cut pLKL67Y were equally reduced in all three of the repair mutants in early stationary phase cells, which contrasted with the early stationary phase results for DSBs with 5' ssDNA overhangs. This could potentially indicate that the Mrx complex plays a role in protection of 3' overhangs in NHEJ repair, which are a favorable substrate for resection nucleases in HDR repair⁵². The Sgs1/Dna2 and Exo1 nucleases act on DSBs with 3' ssDNA tails to lengthen the ssDNA regions in preparation for HDR, making NHEJ impossible (Figure 38)^{16,24}. Although the 3' ssDNA overhangs on the linear plasmid DNAs are only 4 bases long, they may be substrates for the nucleases *in vivo*. Since the plasmids utilized in this assay contain no homology to the chromosomal DNA, resection-induced HDR cannot be completed, eventually leading to the degradation of the plasmid. The hypothesis that Mrx can protect DSBs with 3' tails from other nucleases will be tested in future work. The experiments will use NHEJ plasmid transformation into *exo1* and *sgs1* mutants to uncover if this also has an effect on the NHEJ repair of 3' overhangs. NHEJ repair efficiency was also analyzed in mid-log phase using the plasmid containing DSBs with 3' overhangs. The *yku70*, *dnl4*, and *mre11* strains all showed strong reductions in the mid-log phase assay.

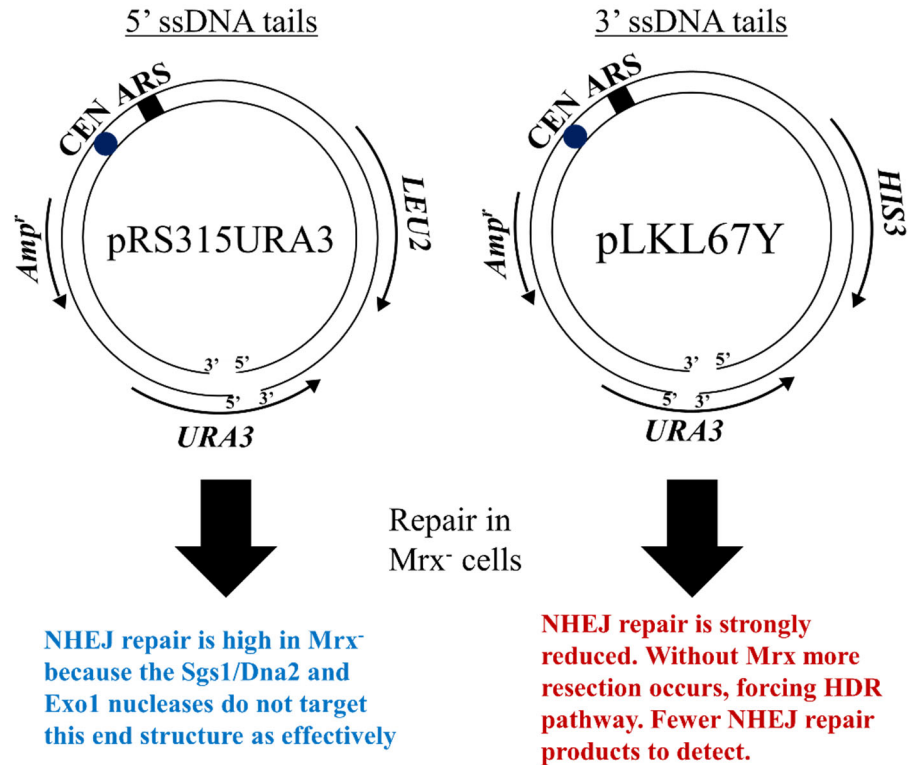


Figure 38. Repair 5' versus 3' ssDNA overhangs in *Mrx*⁻ cells.

The next objective of this study was to analyze the effect of chromatin remodeling on efficient NHEJ repair. Chromatin remodeling proteins facilitate protein access to damaged DNA by adjusting nucleosome positions. A previous study by Jennifer Lilley showed that *arp5* mutants were modestly deficient in NHEJ repair of plasmid DSBs⁴³. Shimada *et al.* also provided evidence that the yeast mutants deficient in the Ino80 remodeling complex were sensitive to reagents that induced DSBs⁴⁶. The first experiment focused on *arp5* cells to reproduce the results found by Jennifer Lilley. The optimized NHEJ plasmid transformation was used and showed that the *arp5* mutant strain was not deficient. The experiment was repeated and no reduction in repair was detected

in *arp5*, *arp6*, or *arp8* mutants. The reason for the conflicting results is unknown, but may be due to technical issues with the protocol that was used.

The last objective of this project was to design a plasmid that enabled the analysis of NHEJ and HDR repair pathways simultaneously. This was accomplished by constructing pLKL103Y from pLKL91Y by inserting additional BsmI and SacI restriction enzyme sites using PCR mutagenesis. When digested with BsmI, this created a gap in the *HIS3* gene which could be repaired using either HDR or NHEJ. When repaired with NHEJ, the plasmid DSB ends were ligated without repairing the missing *HIS3* gap, resulting in the cells becoming Leu⁺His⁻, and unable to grow on Glu-His plates. Cells that utilized HDR accurately repaired the gap in the plasmid, restoring the *HIS3* coding sequence and becoming Leu⁺His⁺. The initial experiment transformed pLKL103Y into wildtype early stationary cells and found that 95% of the repair events utilized the NHEJ pathway. This unexpected result led to the designing of a more flexible plasmid system that could accommodate changes in the location, size, and homology next to the gap region to increase the percentage of cells using homologous recombination for repair.

The next plasmid was created from pLKL91Y by deleting the BspMI Type IIS restriction site via PCR, resulting in the creation of pLKL104Y. Next, two new BspMI sites were added in the *HIS3* gene by PCR to enable the creation of a gapped plasmid with increased sequence homology on the ends. This new approach allows for the ability to produce a gap in different locations in the plasmid depending on where the sites are inserted. Assays with the new gapped plasmid will seek to increase the percentage of cells that use HDR to repair the DSB (Figure 39). This new plasmid increased the sequence homology with the chromosomal DNA to 182 bp on one side and 219 bp on the

other side. Future work will use this unique methodology to analyze yeast strains that are deficient in DNA repair to determine which DSB repair pathways are most defective. This capability is important because some mutants are known to affect both pathways^{55,56}.

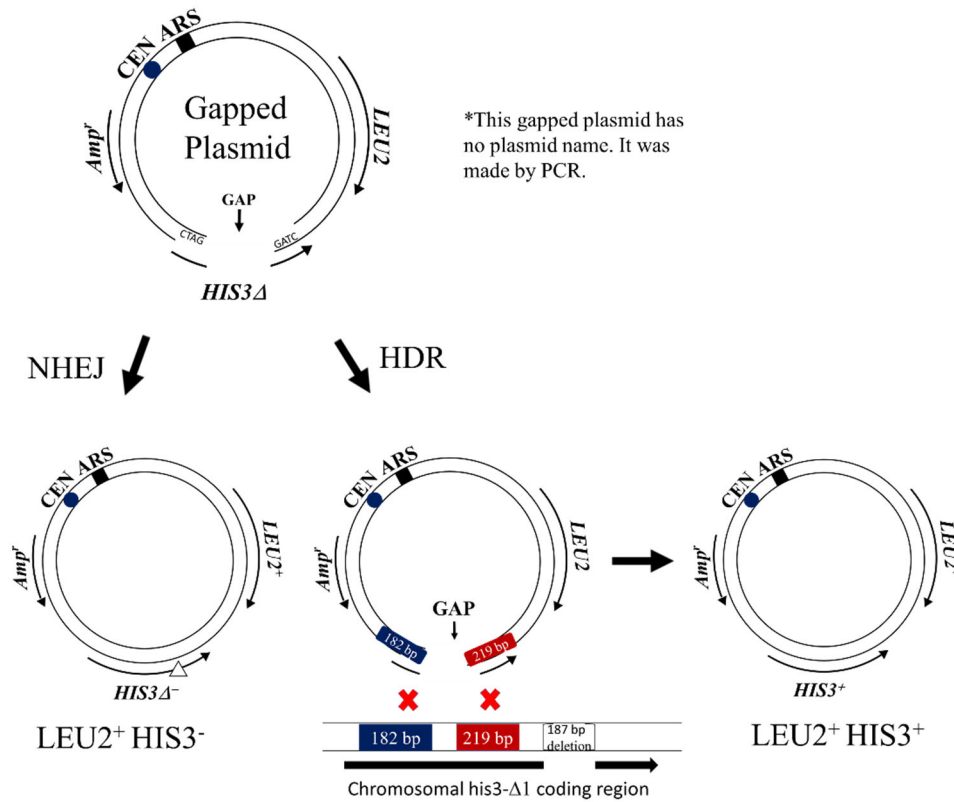


Figure 39. NHEJ vs HDR DSB repair assay diagram using new gapped plasmid system. Gapped plasmid is created by PCR and digested with BspMI as described in Figure 36. The new method introduces a 207 bp gap flanked by two complementary 4 nucleotide 5' overhangs. This gapped plasmid contains additional homology with the chromosome on either side of the gap as well as increased overhang length compared to the pLKL103Y plasmid used in the previous assay.

REFERENCES

1. Jackson, S. P. & Bartek, J. The DNA-damage response in human biology and disease. *Nature* vol. 461 1071–1078 (2009).
2. Barnes, D. E. & Lindahl, T. Repair and Genetic Consequences of Endogenous DNA Base Damage in Mammalian Cells. *Annual Review of Genetics* **38**, 445–476 (2004).
3. Helleday, T., Eshtad, S. & Nik-Zainal, S. Mechanisms underlying mutational signatures in human cancers. *Nature Reviews Genetics* vol. 15 585–598 (2014).
4. D’Andrea, A. D. DNA Repair Pathways and Human Cancer. in *The Molecular Basis of Cancer* 39–55 (Elsevier Inc., 2008). doi:10.1016/B978-141603703-3.10004-4.
5. Cannan, W. J. & Pederson, D. S. Mechanisms and Consequences of Double-Strand DNA Break Formation in Chromatin. *Journal of Cellular Physiology* vol. 231 3–14 (2016).
6. Godet, I. & M. Gilkes, D. BRCA1 and BRCA2 mutations and treatment strategies for breast cancer. *Integrative Cancer Science and Therapeutics* **4**, (2017).
7. Zhu, Y. *et al.* BRCA mutations and survival in breast cancer: An updated systematic review and meta-analysis. *Oncotarget* **7**, 70113–70127 (2016).
8. Holloman, W. K. Unraveling the mechanism of BRCA2 in homologous recombination. *Nature Structural and Molecular Biology* vol. 18 748–754 (2011).

9. Dworaczek, H. & Xiao, W. Xeroderma pigmentosum: A glimpse into nucleotide excision repair, genetic instability, and cancer. *Critical Reviews in Oncogenesis* vol. 13 159–177 (2007).
10. Digiovanna, J. J. & Kraemer, K. H. Shining a light on xeroderma pigmentosum. *Journal of Investigative Dermatology* vol. 132 785–796 (2012).
11. Karahan, B., Argon, A., Yildirim, M. & Vardar, E. Relationship between MLH-1, MSH-2, PMS-2, MSH-6 expression and clinicopathological features in colorectal cancer. *International Journal of Clinical and Experimental Pathology* **8**, 4044–4053 (2015).
12. Daley, J. M. & Sung, P. RIF1 in DNA Break Repair Pathway Choice. *Molecular Cell* vol. 49 840–841 (2013).
13. Shibata, A. *et al.* DNA Double-Strand Break Resection Occurs during Non-homologous End Joining in G1 but Is Distinct from Resection during Homologous Recombination. *Molecular Cell* **65**, 671-684.e5 (2017).
14. Martina, M., Bonetti, D., Villa, M., Lucchini, G. & Longhese, M. P. *Saccharomyces cerevisiae* Rif1 cooperates with MRX-Sae2 in promoting DNA-end resection. *EMBO Reports* **15**, 695–704 (2014).
15. Bonetti, D., Clerici, M., Manfrini, N., Lucchini, G. & Longhese, M. P. The MRX complex plays multiple functions in resection of Yku- and Rif2-protected DNA ends. *PLoS ONE* **5**, e14142 (2010).

16. Daley, J. M., Palmbo, P. L., Wu, D. & Wilson, T. E. Nonhomologous End Joining in Yeast. *Annual Review of Genetics* **39**, 431–451 (2005).
17. Fontana, G. A. *et al.* Rif1 S-acylation mediates DNA double-strand break repair at the inner nuclear membrane. *Nature Communications* **10**, 1–14 (2019).
18. Ghodke, I. & Muniyappa, K. Processing of DNA double-stranded breaks and intermediates of recombination and repair by *Saccharomyces cerevisiae* mre11 and its stimulation by Rad50, Xrs2, and Sae2 proteins. *Journal of Biological Chemistry* **288**, 11273–11286 (2013).
19. Marsella, A., Cassani, C., Casari, E., Tisi, R. & Longhese, M. P. Structure–function relationships of the Mre11 protein in the control of DNA end bridging and processing. *Current Genetics* vol. 65 11–16 (2019).
20. Trujillo, K. M. *et al.* Yeast xrs2 binds DNA and helps target rad50 and mre11 to DNA ends. *The Journal of biological chemistry* **278**, 48957–48964 (2003).
21. Cannavo, E., Cejka, P. & Kowalczykowski, S. C. Relationship of DNA degradation by *Saccharomyces cerevisiae* Exonuclease 1 and its stimulation by RPA and Mre11-Rad50-Xrs2 to DNA end resection. *Proceedings of the National Academy of Sciences of the United States of America* **110**, (2013).
22. Li, X. & Heyer, W. D. Homologous recombination in DNA repair and DNA damage tolerance. *Cell Research* vol. 18 99–113 (2008).
23. Matos, J. & West, S. C. Holliday junction resolution: Regulation in space and time. *DNA Repair* **19**, 176–181 (2014).

24. Chang, H. H. Y., Pannunzio, N. R., Adachi, N. & Lieber, M. R. Non-homologous DNA end joining and alternative pathways to double-strand break repair. *Nature Reviews Molecular Cell Biology* vol. 18 495–506 (2017).
25. Fell, V. L. & Schild-Poulter, C. The Ku heterodimer: Function in DNA repair and beyond. *Mutation Research - Reviews in Mutation Research* vol. 763 15–29 (2015).
26. Shim, E. Y. *et al.* *Saccharomyces cerevisiae* Mre11/Rad50/Xrs2 and Ku proteins regulate association of Exo1 and Dna2 with DNA breaks. *EMBO Journal* **29**, 3370–3380 (2010).
27. Grundy, G. J., Moulding, H. A., Caldecott, K. W. & Rulten, S. L. One ring to bring them all-The role of Ku in mammalian non-homologous end joining. *DNA Repair* **17**, 30–38 (2014).
28. Davis, A. J., Chen, B. P. C. & Chen, D. J. DNA-PK: A dynamic enzyme in a versatile DSB repair pathway. *DNA Repair* **17**, 21–29 (2014).
29. Mimitou, E. P. & Symington, L. S. Ku prevents Exo1 and Sgs1-dependent resection of DNA ends in the absence of a functional MRX complex or Sae2. *EMBO Journal* **29**, 3358–3369 (2010).
30. Altmann, T. & Gennery, A. R. DNA ligase IV syndrome; a review. *Orphanet Journal of Rare Diseases* vol. 11 1–7 (2016).

31. Park, J. *et al.* The DNA Ligase IV Syndrome R278H Mutation Impairs B Lymphopoiesis via Error-Prone Nonhomologous End-Joining. *The Journal of Immunology* **196**, 244–255 (2016).
32. Emerson, C. H. & Bertuch, A. A. Consider the workhorse: Nonhomologous end-joining in budding yeast¹. *Biochemistry and Cell Biology* **94**, 396–406 (2016).
33. Bao, Y. & Shen, X. Chromatin remodeling in DNA double-strand break repair. *Current Opinion in Genetics and Development* vol. 17 126–131 (2007).
34. Langerak, P. & Russell, P. Regulatory networks integrating cell cycle control with DNA damage checkpoints and double-strand break repair. *Philosophical Transactions of the Royal Society B: Biological Sciences* vol. 366 3562–3571 (2011).
35. Ahnesorg, P. & Jackson, S. P. The non-homologous end-joining protein Nej1p is a target of the DNA damage checkpoint. *DNA Repair* **6**, 190–201 (2007).
36. Fell, V. L. & Schild-Poulter, C. Ku Regulates Signaling to DNA Damage Response Pathways through the Ku70 von Willebrand A Domain. *Molecular and Cellular Biology* **32**, 76–87 (2012).
37. Bahmed, K., Seth, A., Nitiss, K. C. & Nitiss, J. L. End-processing during non-homologous end-joining: A role for exonuclease 1. *Nucleic Acids Research* **39**, 970–978 (2011).

38. Chang, H. H. Y. *et al.* Different DNA end configurations dictate which NHEJ components are most important for joining efficiency. *Journal of Biological Chemistry* **291**, 24377–24389 (2016).
39. Lewis, L. K. & Resnick, M. A. Tying up loose ends: Nonhomologous end-joining in *Saccharomyces cerevisiae*. *Mutation Research - Fundamental and Molecular Mechanisms of Mutagenesis* vol. 451 71–89 (2000).
40. Hefferin, M. L. & Tomkinson, A. E. Mechanism of DNA double-strand break repair by non-homologous end joining. *DNA Repair* vol. 4 639–648 (2005).
41. Daley, J. M., Vander Laan, R. L., Suresh, A. & Wilson, T. E. DNA joint dependence of Pol X family polymerase action in nonhomologous end joining. *Journal of Biological Chemistry* **280**, 29030–29037 (2005).
42. Rodriguez, N. D. & Lewis, K. Differential Requirements for Nonhomologous End-joining (NHEJ) Pathway Genes in DNA Repair and Telomere Stability. *The FASEB Journal* **31**, 906.17-906.17 (2017).
43. Jennifer L. Lilley. Analysis of Nhej Dna Repair Efficiency and Accuracy in New. (2015).
44. Van Attikum, H., Fritsch, O. & Gasser, S. M. Distinct roles for SWR1 and INO80 chromatin remodeling complexes at chromosomal double-strand breaks. *EMBO Journal* **26**, 4113–4125 (2007).

45. Van Attikum, H., Fritsch, O., Hohn, B. & Gasser, S. M. Recruitment of the INO80 complex by H2A phosphorylation links ATP-dependent chromatin remodeling with DNA double-strand break repair. *Cell* **119**, 777–788 (2004).
46. Shimada, K. *et al.* Ino80 Chromatin Remodeling Complex Promotes Recovery of Stalled Replication Forks. *Current Biology* **18**, 566–575 (2008).
47. Tripp, J. D., Lilley, J. L., Wood, W. N. & Lewis, L. K. Enhancement of plasmid DNA transformation efficiencies in early stationary-phase yeast cell cultures. *Yeast* **30**, 191–200 (2013).
48. Brachmann, C. B. *et al.* Designer deletion strains derived from *Saccharomyces cerevisiae* S288C: A useful set of strains and plasmids for PCR-mediated gene disruption and other applications. *Yeast* **14**, 115–132 (1998).
49. Sikorski, R. S. & Hieter, P. A system of shuttle vectors and yeast host strains designed for efficient manipulation of DNA in *Saccharomyces cerevisiae*. *Genetics* **122**, 19–27 (1989).
50. Gao, S., Honey, S., Futcher, B. & Grollman, A. P. The non-homologous end-joining pathway of *S. cerevisiae* works effectively in G1-phase cells, and religates cognate ends correctly and non-randomly. *DNA Repair* **42**, 1–10 (2016).
51. Haber, J. E. Mating-type genes and MAT switching in *Saccharomyces cerevisiae*. *Genetics* **191**, 33–64 (2012).

52. Doerfler, L. & Schmidt, K. H. Exo1 phosphorylation status controls the hydroxyurea sensitivity of cells lacking the Pol32 subunit of DNA polymerases delta and zeta. *DNA Repair* **24**, 26–36 (2014).
53. Cannavo, E. *et al.* Regulatory control of DNA end resection by Sae2 phosphorylation. *Nature Communications* **9**, 1–14 (2018).
54. Sorenson, K. S., Mahaney, B. L., Lees-Miller, S. P. & Cobb, J. A. The non-homologous end-joining factor Nej1 inhibits resection mediated by Dna2–Sgs1 nuclease-helicase at DNA double strand breaks. *Journal of Biological Chemistry* **292**, 14576–14586 (2017).
55. Lewis, L. K. *et al.* Role of the Nuclease Activity of *Saccharomyces cerevisiae* Mre11 in Repair of DNA Double-Strand Breaks in Mitotic Cells. *Genetics* (2004) doi:10.1534/genetics.166.4.1701.
56. Lewis, L. K., Karthikeyan, G., Cassiano, J. & Resnick, M. A. Reduction of nucleosome assembly during new DNA synthesis impairs both major pathways of double-strand break repair. *Nucleic Acids Research* (2005) doi:10.1093/nar/gki806.